The Cs 6S-7S-6P3/2 forbidden three-level system : analytical description of the inhibited fluorescence and optical rotation spectra

M. A. Bouchiat, J. Guéna, Ph. Jacquier, M. Lintz, L. Pottier

Classification
Physics Abstracts
32.70 — 32.80 — 33.35 — 35.10W

The Cs 6S-7S-6$P_{3/2}$ forbidden three-level system : analytical description of the inhibited fluorescence and optical rotation spectra

M. A. Bouchiat, J. Guéna, Ph. Jacquier, M. Lintz and L. Pottier

Laboratoire de Spectroscopie Hertzienne (*) de l'Ecole Normale Supérieure, 24 rue Lhomond, F-75231 Paris Cedex 05, France

(*Reçu le 27 mai 1988, accepté le 14 septembre 1988*)

Résumé. — En vue d'améliorer la précision des mesures de violation de parité dans le césium, nous avons étudié le « système interdit à trois niveaux » 6S-7S-6$P_{3/2}$, dans lequel un premier laser excite la transition interdite 6S-7S pendant qu'un deuxième faisceau, colinéaire au premier, sonde les atomes excités dans le niveau 7S. Dans cet article, nous présentons un calcul analytique de la fluorescence du niveau 7S, ainsi que de l'amplification du faisceau sonde, en fonction des fréquences des lasers. Nous prenons en compte les collisions dans le niveau de résonance 6$P_{3/2}$, ainsi que la multiplicité des niveaux et les polarisations des lasers. L'accord quantitatif avec l'expérience est satisfaisant ; les spectres sans effet Doppler sont correctement décrits. Nous obtenons les amortissements de la cohérence 7S-6$P_{3/2}$ et de la population emprisonnée dans 6$P_{3/2}$. Nous présentons de nouveaux procédés de détection de l'orientation du niveau 7S, qui doivent pouvoir être étendus directement à la détection d'un alignement.

Abstract. — With a view to improved parity violation measurements in Cs, we have considered the 6S-7S-6$P_{3/2}$ « forbidden three-level system », in which one laser excites the forbidden 6S-7S transition while a second, colinear laser probes the excited 7S atoms. This paper presents an analytical calculation of the 7S → 6$P_{1/2}$ fluorescence intensity and of the probe amplification as functions of the laser frequencies. The collisional processes in the 6$P_{3/2}$ resonance level, as well as the level multiplicity and the laser polarizations are taken into account. The quantitative agreement with experiment is good ; in particular, the observed sub-Doppler structures are correctly described. The damping rates of the 7S-6$P_{3/2}$ coherence and of the trapped 6$P_{3/2}$ atoms are extracted. New detection schemes for detecting a 7S orientation, with direct possible extension to an alignment, are demonstrated.

1. Introduction.

In recent years, atomic physics parity violation (PV) experiments [1] have contributed to the knowledge of weak interaction processes. Experiments in which a laser beam excites a forbidden transition have succeeded in measuring the so-called « weak charge » of the cesium

(*) Associé au CNRS et à l'université P. et M. Curie.

nucleus. This is the additive parameter, analogous to the electric charge, that characterizes the Z^0-nucleus vector coupling [2, 3]. The result of the measurements [4, 5] matches the prediction of the Standard Model of weak, strong, and electromagnetic interactions.

However, the weak charge is a fundamental parameter. Its value is sensitive to higher order corrections that involve virtual emission or absorption of particles. Measuring the nuclear weak charge of cesium a factor ten more accurately gives access to these corrections, and dramatically changes the significance of the comparison between experiment and theory.

In order to improve the statistical accuracy, the detection of the excited atoms has been reconsidered [6]. Rather than analysing fluorescence light, monitoring a transmitted probe beam allows in principle the detection of all excited atoms, in a single direction and a single transition, thus leading to better detection efficiency. This is the direct motivation for the present work, which deals with the interaction of a vapour with two laser beams : one excites the forbidden 6S-7S transition ; the other probes the final state of the transition. Ultimately, since parity violation takes place in the excitation process, the second laser will serve to detect the resulting breaking of mirror symmetry in the final state.

The present stage is preliminary. It aims at exploring the potentialities of this method and at fully understanding the parity conserving processes in this situation. Since the excitation laser connects two states of the *same* parity, the distribution of parities in this three-level, two-laser system is quite unusual. For that reason we call it a « forbidden three-level system ».

In this paper we present a theoretical approach to the forbidden three-level system formed by Cs vapour in the presence of two resonant single-mode cw lasers, one of which excites the 6S-7S forbidden transition, while the other probes the 7S-$6P_{3/2}$ transition. Agreement with experimental data is illustrated, and damping rates of the system are obtained. Moreover it is shown that even PV measurements *by fluorescence detection* can benefit from the use of the 7S-$6P_{3/2}$ probe.

1.1 THE ATOMIC TRANSITIONS. — As in the previous PV experiments in Cs, a cw laser beam excites the 6S-7S highly forbidden M1 transition (oscillator strength $\simeq 10^{-15}$) in the presence of a transverse electric field $\mathbf{E}_S$ (a few hundred V/cm ; oscillator strength up to 10^{-10}). The 6S and 7S hfs splittings (level diagram in Fig. 1a) are much greater than the Doppler width, and only one component is excited. The Stark-induced E1 transition is described by the scalar and vector polarizabilities α and β ($|\beta| \simeq |\alpha|/10$) [2].

In this paper we first consider an excitation laser of linear polarization $\hat{\varepsilon}_e /\!/ \mathbf{E}_S$; β is not involved, and the only effect of the laser is to bring population in the 7S state. There is no orientation. Later on, when the laser is polarized circularly, we shall deal with a 7S orientation proportional to β/α.

The allowed 7S-$6P_{3/2}$ transition has a large oscillator strength : $\simeq 0.44$. The hfs in $6P_{3/2}$ is only $\simeq 200$ MHz and cannot be resolved in Doppler-broadened spectroscopy. The $7S \rightarrow 6P$ spontaneous emission populates the $6P_{3/2}$ and $6P_{1/2}$ levels with branching ratios of roughly 2/3 and 1/3. The Norcross model [7] predicts 0.649 and 0.351. But to our knowledge there is up to now no precise empirical determination.

1.2 THE FORBIDDEN THREE-LEVEL SYSTEM. — The basic concept of a three-level system driven by two resonant lasers has attracted a great deal of experimental and theoretical efforts in the past twenty years (an excellent list of references can be found in [8]). In spite of the apparent similarity, the forbidden three-level system differs from the systems considered in usual three-level spectroscopy. This results from the unusual distribution of the parities among the system. One obvious difference lies in the very small excitation rate of the forbidden transition, which requires only a lowest order treatment. Furthermore, while the coherent process (here, direct $6S \rightarrow 6P_{3/2}$ two-photon excitation) dominates in usual three-

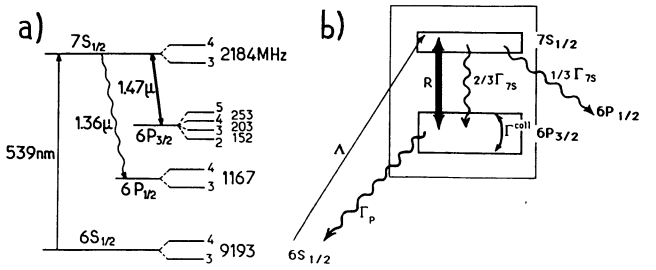

Fig. 1. — a) Relevant energy levels of the Cs atom with their hyperfine structure (not to scale. Natural cesium contains only ^{133}Cs, with $I = 7/2$). b) Radiative and collisional couplings between the levels. Straight lines indicate the laser couplings ; wavy arrows indicate spontaneous emission. The outer box delimits the two-level system mentioned in § 1.2. Precise definitions of the transition and damping rates are given in section 1.2.

level systems, the forbidden three-level system essentially undergoes incoherent stepwise processes (6S→7S absorption, then 7S → 6P$_{3/2}$ induced emission). The efficiency ratio of stepwise to coherent processes is known to be comparable to the ratio Γ_{7S}/Γ_r of the damping rates of the intermediate (7S) level and of the two-photon (6S-6P$_{3/2}$) coherence [9]. The collisional broadening of the 6S-6P resonance lines [10, 11] is known to be very efficient at the Cs densities of interest here (several × 10^{14} at/cm^3), while the 7S level is nearly unaffected by Cs-Cs collisions [12]. As a consequence, the relative contribution of the coherent process is significantly reduced as soon as collisional broadening takes place. In addition, a quantitative calculation shows that the coherent contribution is further reduced by the energy ratio of the forbidden transition to the 7S-6P$_{3/2}$ transition ($\simeq 2.72$). Therefore the contribution of the coherent two-photon process is smaller even at Cs densities low enough for no significant collisional broadening to take place. As a result, the vapour under the action of the two laser beams, behaves merely as a two-level system (the 7S-6P$_{3/2}$ system, outer box in Fig. 1b) coupled to the probe beam. Because of resonance radiation trapping, population escapes this two-level system by 7S → 6P$_{1/2}$ spontaneous decay more easily than by emission of 6P$_{3/2}$ → 6S resonance photons.

1.3 THE MODEL. — In the experiments, both the 7S → 6P$_{1/2}$ fluorescence intensity and the intensity and polarization of the transmitted probe beam have been detected. Special attention has been paid to contributions proportional to the helicity of the excitation beam. All observed signals are calculated below. The hyperfine structure and the collisional redistribution in 6P$_{3/2}$ are taken into account. The following assumptions are made :

i) The two cw single-mode lasers, whose frequency jitters do not contribute to the widths by more than 1 MHz each, are considered to be monochromatic. Their intensity is assumed to be uniform over the volume of vapour.

ii) Each population or coherence is calculated at the lowest non-zero order of the forbidden transition.

iii) The coherent two-photon effect is neglected. The validity of this assumption is checked in appendix A.

iv) The collisional redistribution in the 6P$_{3/2}$ resonance level is described by a collision model where a 6P$_{3/2}$ atom transfers its excitation to a 6S atom while their velocities remain unchanged. After the collision, the distribution of the velocity of the new 6P$_{3/2}$ atom is

therefore assumed to be thermal. This « strong collision » model is a good description of resonance collisions as well as of emission and reabsorption of a resonance photon. Since the collision time is smaller than the inverse $6P_{3/2}$ hfs splitting, the hf momentum is also assumed to be redistributed over all values ($F' = 2$ to 5) with probabilities proportional to the multiplicities $2F' + 1$.

v) The effect of Cs-Cs collisions on 7S atoms is considered to be negligible.

vi) The collisional transfer between $6P_{1/2}$ and $6P_{3/2}$ is neglected (see discussion in § 3.5.2).

vii) Due to the complexity that results from large angular momenta, one has to omit the higher order tensors ($K \geqslant 3$). This approximation restricts to low saturation values ($s \lesssim 1$) the domain of quantitative validity of the solution, but allows an *analytical* treatment to all orders.

viii) The width of the probe transition is considered to be large as compared to the width of the 7S population source, but small as compared to the Doppler width. As long as the saturation broadening remains moderate, the integrations over the velocity distribution then simplify and an analytical solution is obtained.

The good agreement between experimental and theoretical data allows us to extract from theoretical fits the damping rates of the 7S-$6P_{3/2}$ system, and the value of the 7S orientation created by a circularly polarized excitation laser.

2. The atomic evolution in the presence of the two cw resonant lasers.

2.1 FORMULATION OF THE PROBLEM. — We shall develop a semi-classical treatment of the problem. The main notations are illustrated in figure 1b.

2.1.1 *The lasers fields.* — The cw lasers are described by classical fields :

$$\mathcal{E}_j(z, t) = \frac{1}{2}\,\mathcal{E}_j\,\hat{\varepsilon}_j \exp\{-i\,\omega_j(t - z/c)\} + \text{c.c.}\,,$$

where $j = e$ represents the (green) laser exciting one hf component of the 6S-7S transition, and $j = d$ represents the (I.R.) detection laser probing the 7S-$6P_{3/2}$ transition. The 6S→7S transition is highly forbidden, even in the presence of the Stark field. As a result, 7S atomic densities in the experiments remain small. Therefore we neglect in this first stage any alteration in the field amplitude, polarization and phase caused by propagation ; this problem will be treated in section 5.

For an atom of velocity $\mathbf{v}$, the frequencies of the fields in the atom's frame are shifted by longitudinal Doppler effect :

$$\omega_j \to \omega_j - \omega_j(\mathbf{v}\cdot\hat{k})/c\,, \quad j = e \quad \text{or} \quad d\,.$$

We have assumed that the two beams propagate in exactly the same direction of unit vector $\hat{k}$. We define the quantity

$$\nu \equiv \omega_d(\mathbf{v}\cdot\hat{k})/c \tag{1}$$

which is the Doppler shift for the probe beam. From now on, it will be convenient to call « velocity » the quantity ν instead of $\mathbf{v}$. So, for an atom of velocity ν, the time dependence of the laser fields reads

$$\mathcal{E}_e(t, \nu) = \frac{1}{2}\,\mathcal{E}_e\,\hat{\varepsilon}_e \exp\{-i\,(\omega_e - 2.72\,\nu)\,t\} + \text{c.c.} \tag{2a}$$

$$\mathcal{E}_d(t, \nu) = \frac{1}{2}\,\mathcal{E}_d\,\hat{\varepsilon}_d \exp\{-i\,(\omega_d - \nu)\,t\} + \text{c.c.} \tag{2b}$$

The frequency of the probe beam is swept over frequency intervals of at most 3 GHz, so that in practice ω_e/ω_d never deviates from the approximate value 2.72.

2.1.2 *The cesium vapour.* — Each velocity class of the atoms in the vapour is described (in the interaction representation) by a density matrix $\rho(v)$. The number of Cs atoms per unit volume whose velocity lies between v and $v + dv$ is tr $\{\rho(v)\}\, dv$. Finally only the subspace spanned by the $6S_{1/2}F$, $7S_{1/2}F$, and $6P_{3/2}F'$ levels ([1]) is considered.

2.1.2.1 The populations and their relaxation. — Using the notation $\mathbb{P}(\alpha F) \equiv \sum_m |\alpha, Fm\rangle \langle \alpha, Fm|$ for the projector over the αF hfs level, we define the density matrices and the populations of the involved levels by :

$$\rho_{6F}(v) \equiv \mathbb{P}(6S_{1/2}F)\,\rho(v)\,\mathbb{P}(6S_{1/2}F) \qquad n_{6F}(v) \equiv \text{tr}\,\{\rho_{6F}(v)\}$$
$$\rho_{7F}(v) \equiv \mathbb{P}(7S_{1/2}F)\,\rho(v)\,\mathbb{P}(7S_{1/2}F) \qquad n_{7F}(v) \equiv \text{tr}\,\{\rho_{7F}(v)\}$$
$$\rho_{PF'}(v) \equiv \mathbb{P}(6P_{3/2}F')\,\rho(v)\,\mathbb{P}(6P_{3/2}F') \qquad n_{PF'}(v) \equiv \text{tr}\,\{\rho_{PF'}(v)\}\ .$$

Since the fraction of excited atoms is always very small, the ground state remains thermally populated and we can write :

$$\rho_{6F}(v) = \frac{\mathbb{P}(6S_{1/2}F)}{2(2I+1)}\, f(v)\, n_{Cs}\ .$$

Here $I = 7/2$ is the nuclear spin of ^{133}Cs ; n_{Cs} is the atomic Cs density and

$$f(v) = (1/\Omega_D \sqrt{2\pi}) \exp\{-v^2/(2\,\Omega_D^2)\} \tag{3}$$

is the normalized Boltzmann velocity distribution ; $\Omega_D \equiv \omega_{7S\text{-}6P_{3/2}} \sqrt{kT/M_{Cs}\,c^2}$ is the Doppler half-width at $1/\sqrt{e}$ ($\simeq 2\pi \times 110$ MHz for the temperatures of interest here).

The only relaxation process in the 7S state is the radiative 7S → 6P decay :

$$\dot{\rho}_{7F}(v)\big|_{rel} = -\,\Gamma_{7S}\,\rho_{7F}(v)\ ; \tag{4}$$

where $1/\Gamma_{7S} = 48$ ns is the radiative lifetime of the 7S level [12]. The same relation holds for $n_{7F}(v)$.

For the resonant $6P_{3/2}$ states, on the contrary, resonant collisions as well as resonance radiation trapping have to be taken into account. The equation that governs the evolution of the population under relaxation contains several contributions :

$$\dot{n}_{PF'}(v)\big|_{rel} = \sum_F \frac{2}{3}\,\Gamma_{7S}\,C_{F'}^{F}\,n_{7F}(v) - \Gamma_P\,n_{PF'}(v) + \Gamma^{coll}(w_{F'}\,f(v)\,\bar{n}_P - n_{PF'}(v))\ . \tag{5}$$

The first term describes the 7S → $6P_{3/2}$ spontaneous emission. For the branching ratios of the 7S → $6P_{3/2}$ and 7S → $6P_{1/2}$ fluorescence we use the values 2/3 and 1/3 (which take no account of spin-orbit effects). The relative oscillator strengths $C_{F'}^{F}$ are defined so that $\sum_{F'} C_{F'}^{F} = 1$ (App. B).

([1]) The hyperfine momentum is indicated by F (= 3 or 4) in the 6S and 7S levels, and by F' (= 2, 3, 4, or 5) in the $6P_{3/2}$ levels.

The second term describes the global decay of the $6P_{3/2}$ population. Because of radiation trapping, the rate Γ_P is much less than the radiative decay rate of an isolated $6P_{3/2}$ atom [13] (typically by two orders of magnitude, as shown in our data analysis, given below).

The third term of equation (5), in which

$$\bar{n}_P = \sum_{F'} \left\{ \int_{-\infty}^{+\infty} n_{PF'}(\nu)\, d\nu \right\} \tag{6}$$

is the total $6P_{3/2}$ population, and

$$w_{F'} = (2F' + 1)/\sum_{F''} (2F'' + 1) = (2F' + 1)/32 \tag{7}$$

the relative degeneracy of the $6P_{3/2}F'$ level, describes the redistribution of the $6P_{3/2}$ atoms over all thermal velocities and over all hfs levels. One can easily check that the third term does not give rise to any global decay of the $6P_{3/2}$ population. On the other hand, a velocity class relaxes with a rate $\Gamma_P + \Gamma^{coll}$.

2.1.2.2 The coherences and their relaxation. — The 6S-7S coherences $\rho_{6F\text{-}7F}(\nu) \equiv \mathbb{P}(6SF)\, \rho(\nu)\, \mathbb{P}(7SF)$ undergo only radiative decay :

$$\dot{\rho}_{6F\text{-}7F}(\nu)\big|_{rel} = -(\Gamma_{7S}/2)\, \rho_{6F\text{-}7F}(\nu)$$

while the 7S-$6P_{3/2}$ coherences

$$\rho_{FF'}(\nu) \equiv \mathbb{P}(7SF)\, \rho(\nu)\, \mathbb{P}(6P_{3/2}F')$$

are damped

$$\dot{\rho}_{FF'}(\nu)\big|_{rel} = -\gamma \rho_{FF'}(\nu)$$

with a rate γ which reflects both radiative and collisional processes.

2.2 THE MASTER EQUATION AND THE STEPWISE APPROXIMATION. — For the class of velocity ν, the evolution of the density matrix is given by

$$\dot{\rho}(\nu) = -\frac{i}{\hbar}[\mathcal{H}(t, \nu), \rho(\nu)] + \dot{\rho}(\nu)\big|_{rel}$$

where $\mathcal{H}(t, \nu)$ is the Hamiltonian for the atom-field coupling in the interaction representation :

$$\mathcal{H}(t, \nu) = -\left\{ e^{i\mathcal{H}_0 t/\hbar} \mathfrak{D}\, e^{-i\mathcal{H}_0 t/\hbar} \right\} \cdot \{\mathfrak{E}_e(t, \nu) + \mathfrak{E}_d(t, \nu)\}$$

($\mathfrak{D}$ is the electric dipole operator, $\mathcal{H}_0$ the Hamiltonian of an atom in the Stark field). Applying the rotating wave approximation, we neglect the non-resonant terms in the matrix elements of $\mathcal{H}(t, \nu)$, that is, the coupling between atomic states for which the detuning is much greater than the Doppler width (all other widths are smaller than Ω_D). We obtain

$$\mathcal{H}(t, \nu) = -\frac{1}{2} \mathfrak{E}_e\, \mathbb{P}(7S_{1/2}\, F)\, \mathfrak{D} \cdot \hat{\varepsilon}_e\, \mathbb{P}(6S_{1/2}\, F)\, e^{2.72\, i(\nu - \nu_e)t} + \text{h.c.} -$$

$$-\frac{1}{2} \mathfrak{E}_d\, \mathbb{P}(7S_{1/2}\, F)\, \mathfrak{D} \cdot \hat{\varepsilon}_d \sum_{F'} \mathbb{P}(6P_{3/2}\, F')\, e^{i(\omega_{FF'} - \omega_d + \nu)t} + \text{h.c.}$$

where $v_e \equiv \{\omega_e - (E_{7SF} - E_{6SF})/\hbar\}/2.72$ is the velocity of the atoms resonant with the green (excitation) laser, and $\omega_{FF'} \equiv (E_{7SF} - E_{6P\,3/2,\,F'})/\hbar$. Here we assume that the two lasers are resonant for the *same* 7SF level (the opposite case will be studied in § 3.3) and that the green laser drives a $\Delta F = 0$ transition.

As indicated in section 1, we shall neglect the 6S-6P two-photon coherence (except in appendix A where the validity of the approximation is checked). The first stage of the step-by-step excitation involves the 6S → 7S transition. In view of its high forbiddenness (oscillator strength $\leq 10^{-9}$ for electric fields $E_S \leq 1\,000$ V/cm), a lowest order calculation is fully appropriate. The green laser is represented by a source term for the 7SF population. This term is :

$$\Lambda_F(v) = n_{6F}(v)\left\{2\left(\frac{d\mathcal{E}_e}{2\hbar}\right)^2 \times \left(\frac{2}{\Gamma_{7S}}\right)\right\} \times \left\{1 + \left(\frac{2.72(v - v_e)}{\Gamma_{7S}/2}\right)^2\right\}^{-1} \tag{8a}$$

where $n_{6F}(v) = n_{Cs}\, f(v)\,(2F + 1)/2(2I + 1)$. The transition dipole matrix element d is defined as $d \equiv \langle \widetilde{6F, Fm} |\, \mathfrak{D} \cdot \hat{\varepsilon}_e \,| \widetilde{7S, Fm} \rangle$ where $|\widetilde{\alpha, Fm}\rangle$ denotes the states in the presence of the Stark field. We assume $\hat{\varepsilon}_e \,/\!/\, \mathbf{E}_S$, so that d involves only the scalar polarizability : $d = \alpha\,|\mathbf{E}_S \cdot \hat{\varepsilon}_e| = \alpha E_S$; the vector polarizability β plays no rôle. (The case of circular polarization will be treated in section 4.) The quantity d is then independent of m. We do not give the details of the calculation leading to equation (8a) since it is very similar to the calculation leading to the coupling with the probe laser (Eq. (14)).

The source term turns out to be the product of a sharp lorentzian shape and a much broader gaussian shape $f(v)$. To a good accuracy, we may replace v by v_e in the gaussian $n_{6F}(v)$ factor and rewrite equation (8a) as

$$\Lambda_F(v) = \Lambda \times g(v)\,, \quad \text{with} \quad \int g(v)\,dv = 1\,, \tag{8b}$$

where the total excitation rate Λ is a constant and $g(v)$ is a normalized lorentzian function.

Now we just have to solve the master equation for the density matrix restricted to the 7S and 6P$_{3/2}$ levels. Defining $\mathfrak{D}_{FF'} \equiv \mathbb{P}(7SF)\,\mathfrak{D} \cdot \hat{\varepsilon}_d\,\mathbb{P}(6P_{3/2}\,F')$, this equation becomes

$$\dot{\rho}(v) = \dot{\rho}(v)|_{rel} + \Lambda g(v)\frac{\mathbb{P}(7SF)}{2F + 1} - \frac{i}{\hbar}\sum_{F'}\left[-\frac{1}{2}\mathcal{E}_d\,\mathfrak{D}_{FF'}\,e^{i(\omega_{FF'} - \omega_d + v)t} + \text{h.c.}, \rho(v)\right]. \tag{9}$$

2.3 THE ATOMIC DENSITY MATRIX IN STEADY STATE. — Let us derive, from equation (9), the equations governing the evolution of the coherences and the populations :

$$\dot{\rho}_{FF'}(v) = -\gamma\rho_{FF'}(v) + \frac{i\mathcal{E}_d}{2\hbar}e^{i(\omega_{FF'} - \omega_d + v)t}\{\mathfrak{D}_{FF'}(v)\,\rho_{PF'}(v) - \rho_{7F}(v)\,\mathfrak{D}_{FF'}\} \tag{10}$$

$$\dot{n}_{7F}(v) = -\Gamma_{7S}\,n_{7F}(v) + \Lambda g(v) + \sum_{F'}\left\{\frac{i\mathcal{E}_d}{2\hbar}e^{i(\omega_{FF'} - \omega_d + v)t}\,\text{tr}\,[\mathfrak{D}_{FF'}\,\rho^{\dagger}_{FF'}(v)] + \text{c.c.}\right\} \tag{11}$$

$$\dot{n}_{PF'}(v) = -(\Gamma_P + \Gamma^{coll})\,n_{PF'}(v) + \Gamma^{coll}\,w_{F'}\,f(v)\,\bar{n}_P + \frac{2}{3}\Gamma_{7S}\,C^F_{F'}\,n_{7F}(v) + \\ + \left\{\frac{i\mathcal{E}^*_d}{2\hbar}e^{-i(\omega_{FF'} - \omega_d + v)t}\,\text{tr}\,[\mathfrak{D}^{\dagger}_{FF'}\,\rho_{FF'}(v)] + \text{c.c.}\right\}. \tag{12}$$

We are interested in the *steady state* of the vapour, for which the populations are constant in time and the coherences $\rho_{FF'}(v)$ oscillate like $e^{i(\omega_{FF'} - \omega_d + v)t}$. Any other term would bring

oscillatory terms in the right hand side of equations (11) and (12). Then, from equation (10), one easily gets an expression for the coherences :

$$\rho_{FF'}(\nu) = \frac{i\mathcal{E}_d}{2\hbar} \frac{e^{i(\omega_{FF'} - \omega_d + \nu)t}}{i(\omega_{FF'} - \omega_d + \nu) + \gamma} \{\mathfrak{D}_{FF'} \rho_{PF'}(\nu) - \rho_{7F}(\nu) \mathfrak{D}_{FF'}\} , \tag{13}$$

which can be carried back in equations (11) and (12). Finally the steady-state equations for the 7S and $6P_{3/2}$ populations are

$$0 = - \Gamma_{7S} n_{7F}(\nu) + \Lambda g(\nu) + \sum_{F'} \frac{(2/\gamma)|\mathcal{E}_d/2\hbar|^2}{1 + \Delta_{F'}^{\nu 2}} \text{ tr } \{\mathfrak{D}_{FF'}^{\dagger} \mathfrak{D}_{FF'} \rho_{PF'}(\nu) - \mathfrak{D}_{FF'} \mathfrak{D}_{FF'}^{\dagger} \rho_{7F}(\nu)\} \tag{14}$$

$$0 = - (\Gamma_P + \Gamma^{coll}) n_{PF'}(\nu) + \Gamma^{coll} w_{F'} f(\nu) \bar{n}_P + \frac{2}{3} \Gamma_{7S} C_{F'}^{F} n_{7F}(\nu) + \sum_{F'} \frac{(2/\gamma)|\mathcal{E}_d/2\hbar|^2}{1 + \Delta_{F'}^{\nu 2}} \text{ tr } \{\mathfrak{D}_{FF'} \mathfrak{D}_{FF'}^{\dagger} \rho_{7F}(\nu) - \mathfrak{D}_{FF'}^{\dagger} \mathfrak{D}_{FF'} \rho_{PF'}(\nu)\} \tag{15}$$

where we have introduced the notation $\Delta_{F'}^{\nu} \equiv (\omega_{FF'} - \omega_d + \nu)/\gamma$.

In equations (14), (15), it appears that the steady-state populations are not only coupled to the populations, but also to other elements of the density matrices of the 7S and $6P_{3/2}$ levels. Writing a detailed expression for the operators $\mathfrak{D}_{FF'} \mathfrak{D}_{FF'}^{\dagger}$ (which acts on the 7SF level) and $\mathfrak{D}_{FF'}^{\dagger} \mathfrak{D}_{FF'}$ (which acts on the $6P_{3/2}$ F' level) will clarify the couplings between populations, orientations, alignments, etc...

2.4 THE COUPLINGS OF POPULATION TO ORIENTATION AND ALIGNMENT. — Let us consider two tensor operators $\vec{\mathcal{C}}^{F}_{F'} \downarrow$ and $\vec{\mathcal{C}}^{F}_{F'} \uparrow$ of rank 2, such that for any two vectors **u**, **v**, the following relations hold :

$$\mathbf{u} \cdot \vec{\mathcal{C}}^{F}_{F'} \downarrow \cdot \mathbf{v} = \mathbb{P}(7SF)\, \mathfrak{D} \cdot \mathbf{u}\, \mathbb{P}(6P_{3/2}\, F')\, \mathfrak{D} \cdot \mathbf{v}\, \mathbb{P}(7SF) \tag{16}$$

$$\mathbf{u} \cdot \vec{\mathcal{C}}^{F}_{F'} \uparrow \cdot \mathbf{v} = \mathbb{P}(6P_{3/2}\, F')\, \mathfrak{D} \cdot \mathbf{u}\, \mathbb{P}(7SF)\, \mathfrak{D} \cdot \mathbf{v}\, \mathbb{P}(6P_{3/2}\, F') . \tag{17}$$

Then one has $\mathfrak{D}_{FF'} \mathfrak{D}_{FF'}^{\dagger} = \hat{\varepsilon}_d \cdot \vec{\mathcal{C}}^{F}_{F'} \downarrow \hat{\varepsilon}_d^{*}$. In Appendix B we have performed the decomposition of $\vec{\mathcal{C}} \downarrow$ and $\vec{\mathcal{C}} \uparrow$ on the basis of the irreducible tensor operators $\vec{\mathbf{F}}^{(0)}$, $\vec{\mathbf{F}}^{(1)}$, and $\vec{\mathbf{F}}^{(2)}$, of ranks 0, 1, and 2, defined by

$$\mathbf{u} \cdot \vec{\mathbf{F}}^{(0)} \cdot \mathbf{v} = (\mathbf{F}^2/3)\, (\mathbf{u} \cdot \mathbf{v}) \tag{18a}$$

$$\mathbf{u} \cdot \vec{\mathbf{F}}^{(1)} \cdot \mathbf{v} = (1/2)\, \mathbf{F} \cdot (\mathbf{u} \wedge \mathbf{v}) \tag{18b}$$

$$\mathbf{u} \cdot \vec{\mathbf{F}}^{(2)} \cdot \mathbf{v} = (1/2)\, [(\mathbf{F} \cdot \mathbf{u})\, (\mathbf{F} \cdot \mathbf{v}) + (\mathbf{F} \cdot \mathbf{v})\, (\mathbf{F} \cdot \mathbf{u})] - (\mathbf{F}^2/3)\, (\mathbf{u} \cdot \mathbf{v}) . \tag{18c}$$

The decomposition of $\vec{\mathcal{C}}\downarrow$ reads :

$$\vec{\mathcal{C}}\underset{F'}{\overset{F}{\downarrow}} = C^{F}_{F'} \,|\, \langle 7S_{1/2} \| \mathfrak{D} \| 6P_{3/2} \rangle \,|^2 \times \frac{\mathbb{P}(7SF)}{2F(F+1)} \left\{ \vec{F}^{(0)} + ia \underset{F'}{\overset{F}{\downarrow}} \vec{F}^{(1)} + b \underset{F'}{\overset{F}{\downarrow}} \vec{F}^{(2)} \right\} . \quad (19)$$

The coefficients C, $a\downarrow$, $b\downarrow$ (and the corresponding coefficients $a\uparrow$ and $b\uparrow$ in the decomposition of $\vec{\mathcal{C}}\uparrow$) are given in § 2 of Appendix B. This results in a convenient expression for the operator $\mathfrak{D}_{FF'}\,\mathfrak{D}^{\dagger}_{FF'}$:

$$\mathfrak{D}_{FF'}\,\mathfrak{D}^{\dagger}_{FF'} = C^{F}_{F'} \,|\, \langle 7S_{1/2} \| \mathfrak{D} \| 6P_{3/2} \rangle \,|^2 \frac{\mathbb{P}(7SF)}{2F(F+1)} \times$$

$$\times \left\{ \frac{\mathbf{F}^2}{3} + \frac{i}{2} a \underset{F'}{\overset{F}{\downarrow}} \mathbf{F} \cdot (\hat{\varepsilon}_d \wedge \hat{\varepsilon}_d^*) + b \underset{F'}{\overset{F}{\downarrow}} \hat{\varepsilon}_d \cdot \vec{F}^{(2)} \cdot \hat{\varepsilon}_d^* \right\} . \quad (20)$$

According to equations (14), (15) the observable quantities coupled to the populations are Tr $\{\mathfrak{D}_{FF'}\,\mathfrak{D}^{\dagger}_{FF'}\,\rho_{7F}(\nu)\}$ and the analogous quantity involving $\rho_{PF'}(\nu)$. Using equation (20) it is reexpressed as a combination of three terms : i) Tr $\left\{ \frac{F(F+1)}{3} \rho_{7F}(\nu) \right\} \propto n_{7F}(\nu)$: the probe beam couples the populations, independent of its polarization. ii) Tr $\{\mathbf{F} \cdot (\hat{\varepsilon}_d \wedge \hat{\varepsilon}_d^*)\,\rho_{7F}(\nu)\}$: if the probe is circularly or elliptically polarized, it couples the populations to the orientation. iii)

$$\mathrm{Tr} \left\{ \left[\frac{(\mathbf{F} \cdot \hat{\varepsilon}_d)\,(\mathbf{F} \cdot \hat{\varepsilon}_d^*) + \mathrm{h.c.}}{2} - \frac{\mathbf{F}^2}{3} \right] \rho_{7F}(\nu) \right\} :$$

the alignment along $\hat{\varepsilon}_d$ is also coupled to the populations.

In some of our experiments, the probe beam was circularly polarized [14] ; the corresponding calculation is developed in section 4. Here, with a view to interpreting all spectra recorded with a linearly polarized probe beam, the population-orientation coupling will be omitted. Although the green laser does not create any alignment in the geometrical configuration considered here, yet the alignment may not be *a priori* neglected. The reason is that the probe beam, when it saturates the 7S-6P$_{3/2}$ transition, creates an alignment in the 7S level ([2]). The alignment itself is coupled to the rank-4 tensor and the exact solution would require to take into account all the even rank tensors.

All the spectra from which quantitative values have been extracted were obtained with a weakly saturating probe beam. As shown more explicitly in section 4, it is then justified to restrict ourselves to an approximate solution which omits the alignment and results in important simplifications. Actually, as will appear in section 4, we have been able to take into account the laser-induced alignment (but not the higher-order tensors). The corresponding correction to the spectral shape is less than 10 % for the saturation levels of the experiments (see Fig. 2). No qualitative modification results, even for strong saturation.

Neglecting the alignment we write

$$\rho_{7F}(\nu) = n_{7F}(\nu)\,\mathbb{P}(7SF)/(2F+1)$$

and

$$\rho_{PF'}(\nu) = n_{PF'}(\nu)\,\mathbb{P}(6P_{3/2}\,F')/(2F'+1) .$$

([2]) So does it in the 6P$_{3/2}$ level as well ; but all tensor quantities in the 6P levels are quickly washed off by resonant collisions.

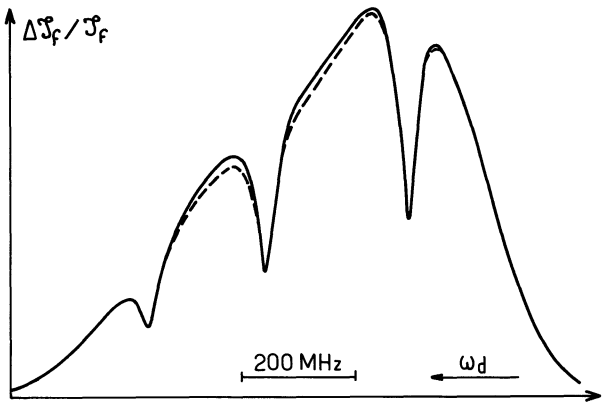

Fig. 2. — Fractional increase of fluorescence caused by the probe beam, *versus* probe frequency. Example spectra calculated without (solid line) or with (dashed line) the alignment-induced corrections. Values of the parameters : $s = 0.8$; $\gamma/2\pi = 18$ MHz ; $\Gamma^{coll}/2\pi = 36$ MHz ; $\Gamma_{P/2\pi} = 100$ kHz.

This gives

$$\mathrm{Tr}\ \{\mathfrak{D}_{FF'}\ \mathfrak{D}^{\dagger}_{FF'}\ \rho_{7F}(\nu)\} = C^{F}_{F'}\ \frac{|\langle 7S_{1/2}\|\ \mathfrak{D}\ \|6P_{3/2}\rangle|^2}{6}\ n_{7F}(\nu) \tag{21}$$

$$\mathrm{Tr}\ \{\mathfrak{D}^{\dagger}_{FF'}\ \mathfrak{D}_{FF'}\ \rho_{PF'}(\nu)\} = \mu^{F}_{F'}\ C^{F}_{F'}\ \frac{|\langle 7S_{1/2}\|\ \mathfrak{D}\ \|6P_{3/2}\rangle|^2}{6}\ n_{PF'}(\nu)$$

where $$\mu^{F}_{F'} \equiv (2F+1)/(2F'+1)\,. \tag{22}$$

To conclude this section, we can now write the steady-state equations for the 7SF and the four $6P_{3/2}\,F'$ populations :

$$\sum_{F'} R^{F}_{F'}(\nu)\ \{\mu^{F}_{F'}\ n_{PF'}(\nu) - n_{7F}(\nu)\} - \Gamma_{7S}\ n_{7F}(\nu) = -\ \Lambda g\,(\nu) \tag{23}$$

$$R^{F}_{F'}(\nu)\ \{n_{7F}(\nu) - \mu^{F}_{F'}\ n_{PF'}(\nu)\} + \frac{2}{3}\Gamma_{7S}\ C^{F}_{F'}\ n_{7F}(\nu) - \\ - (\Gamma_P + \Gamma^{coll})\ n_{PF'}(\nu) + \Gamma^{coll}\ w_{F'}\ f(\nu)\ \bar{n}_P = 0 \tag{24}$$

where we have introduced

$$R^{F}_{F'}(\nu) = C^{F}_{F'}\ \frac{\Omega^2_R}{2\gamma} \times \frac{1}{1+\Delta^{\nu 2}_{F'}}\,.$$

The quantity $\Omega_R = \left|\mathcal{E}_d \langle 7S_{1/2}\|\ \mathfrak{D}\ \|6P_{3/2}\rangle/\hbar\sqrt{6}\right|$ is the « Rabi pulsation » for the 7S-$6P_{3/2}$ transition. Note that the Rabi pulsation for a particular $7SF \rightarrow 6P_{3/2}\,F'$ transition is actually $\Omega_R \sqrt{C^{F}_{F'}}$. Since $C^{F}_{F'}$ ranges from 0.10 to 0.61, we expect different saturation levels from one hfs component to another. (On the other hand, neglecting the alignment, we are led to neglect the variations of the Rabi pulsations associated with different Zeeman components belonging to the same hfs component).

3. Calculation of the « inhibited fluorescence » spectra.

Starting from equations (23) and (24) we are now going to calculate the total 7S population in order to obtain the 7S $\rightarrow$ 6P$_{1/2}$ fluorescence in the presence of the probe beam.

3.1 CALCULATION AT THE LOWEST ORDER IN THE PROBE INTENSITY. — In absence of the probe beam ($R_{F'}^{F}(\nu) = 0$), the expression $n_{7F}^{(0)}(\nu) = \Lambda g(\nu)/\Gamma_{7S}$ for the 7S population can be inserted in equation (24) to obtain :

$$n_{PF'}^{(0)}(\nu) = \frac{2}{3}\Lambda\left\{\frac{\Gamma^{coll}}{\Gamma_P(\Gamma_P + \Gamma^{coll})} w_{F'} f(\nu) + \frac{C_{F'}^{F}}{\Gamma_P + \Gamma^{coll}} g(\nu)\right\} .$$

Next we get the modification of the 7S population to first order in $R_{F'}^{F}(\nu)$:

$$\Delta n_{7F}^{(1)}(\nu) = \sum_{F'} R_{F'}^{F}(\nu)\ \{\mu_{F'}^{F}\, n_{PF'}^{(0)}(\nu) - n_{7F}^{(0)}(\nu)\}/\Gamma_{7S}$$

and the resulting increase of the 7S $\rightarrow$ 6P$_{1/2}$ fluorescence :

$$\begin{aligned}\Delta\mathfrak{J}_f^{(1)}(\omega_d)/\mathfrak{J}_f^{(0)} &= \int \Delta n_{7F}^{(1)}(\nu)\,d\nu \Big/ \int n_{7F}^{(0)}(\nu)\,d\nu \\ &= \sum_{F'}\left\{\frac{2}{3}\frac{\mu_{F'}^{F} w_{F'} \Gamma^{coll}}{\Gamma_P(\Gamma_P + \Gamma^{coll})}\int_{-\infty}^{+\infty} R_{F'}^{F}(\nu) f(\nu)\,d\nu \right. \\ &\quad \left. - \frac{1}{\Gamma_{7S}}\left(1 - \frac{2}{3}\frac{\mu_{F'}^{F} C_{F'}^{F} \Gamma_{7S}}{\Gamma_P + \Gamma^{coll}}\right)\int_{-\infty}^{+\infty} R_{F'}^{F}(\nu) g(\nu)\,d\nu\right\}\end{aligned}$$

This expression involves two different integrals. Instead of a numerical study (the first integral cannot be expressed analytically) we shall use an approximation. Taking advantage of the hierarchy between the half-widths of $g(\nu)$, $R_{F'}^{F}(\nu)$, and $f(\nu)$

$$\left(\frac{1}{2\pi}\frac{\Gamma_{7S}}{2\times 2.72} = 0.6\text{ MHz}\right) \ll \left(\frac{\gamma}{2\pi} = 5\text{ to }40\text{ MHz}\right) \ll \left(\frac{\Omega_D\sqrt{2\ln 2}}{2\pi} \simeq 130\text{ MHz}\right),$$

we consider that $R_{F'}^{F}(\nu)$ is broad as compared to $g(\nu)$, but sharp as compared to $f(\nu)$. Then the integrations are carried out easily by treating the sharper factor as a δ-function :

$$\int_{-\infty}^{+\infty} g(\nu)\, R_{F'}^{F}(\nu)\,d\nu = R_{F'}^{F}(\nu_e) \tag{25a}$$

$$\int_{-\infty}^{+\infty} R_{F'}^{F}(\nu)\, f(\nu)\,d\nu = \frac{\pi C_{F'}^{F}\,\Omega_R^2}{2} f(\omega_{FF'} - \omega_d) . \tag{25b}$$

In addition to the usual saturation parameter

$$s = \Omega_R^2/(2\,\gamma\Gamma_{7S}) , \tag{26a}$$

we shall introduce two dimensionless parameters :

$$\kappa \equiv \Gamma_{7S}/(\Gamma_P + \Gamma^{coll}) , \tag{26b}$$

and the « contrast » parameter

$$\mathcal{C} \equiv \frac{3}{2}\sqrt{\frac{2}{\pi}}\frac{\Gamma_P\,\Omega_D}{\gamma\Gamma_{7S}}. \tag{26c}$$

Finally, at the lowest order, we write the increase of fluorescence

$$\frac{\Delta\mathcal{J}_f^{(1)}(\omega_d)}{\mathcal{J}_f^{(0)}} = \sum_{F'} sC_{F'}^{F}\left\{\frac{-\left[1-\frac{2}{3}\kappa\mu_{F'}^{F}C_{F'}^{F}\right]}{1+\left(\frac{\omega_{FF'}-\omega_d+\nu_e}{\gamma}\right)^2}+\frac{\mu_{F'}^{F}w_{F'}}{\mathcal{C}}\frac{\Gamma^{coll}}{\Gamma_P+\Gamma^{coll}}e^{\frac{-(\omega_{FF'}-\omega_d)^2}{2\Omega_D^2}}\right\}, \tag{27}$$

where the summation $\sum_{F'}$ reduces to three terms ($C_{F'}^{F} = 0$ for $F' = F \pm 2$), corresponding to the three dipole-allowed transitions from the populated 7SF level to the $6P_{3/2}F'$ levels.

Interpretation. — The fluorescence increase (as a function of ω_d) is the sum of sharp, negative lorentzian terms, and of broad, positive, gaussian-shaped terms. The sharp holes reflects « inhibition » (actually reduction) of the fluorescence intensity due to the competition of stimulated emission (« inhibited fluorescence » holes). The broad contribution corresponds to the reexcitation of the population trapped in the $6P_{3/2}$ resonance level. These reexcited atoms get a new chance to be observed in spontaneous decay.

The holes are not exactly centered on the frequencies $\omega_{FF'}/2\pi$ of the $7SF \rightarrow 6P_{3/2}F'$ transitions, but are all Doppler-shifted by a quantity $\nu_e/2\pi$ proportional to the velocity of the atoms excited in the forbidden transition. The hole depth is affected by a factor $1 - 2\,\kappa C_{F'}^{F}\,\mu_{F'}^{F}/3$: this accounts for the presence of velocity-selected atoms in the $6P_{3/2}$ levels caused by spontaneous decay of the 7S atoms. Since $\kappa \ll 1$ (Eq. (26b)), this factor actually remains close to unity, except at very low Cs pressure.

We define the « contrast » of the spectra as the ratio of the hole depth to the height of the corresponding Doppler line. Omitting the factor $\Gamma^{coll}/(\Gamma_P + \Gamma^{coll})$, very close to one since $\Gamma_P \ll \Gamma^{coll}$, the contrast is $\mathcal{C}/\mu_{F'}^{F}\,w_{F'} = \mathcal{C} \times 32/(2F+1)$. It does not depend on F'.

3.2 NON-PERTURBATIVE SOLUTION. — First subtracting equation (24) (summed over F') from equation (23), we get

$$\frac{1}{3}\Gamma_{7S}\,n_{7F}(\nu) + (\Gamma_P + \Gamma^{coll})\sum_{F'} n_{PF'}(\nu) - \Gamma^{coll}\,f(\nu)\,\bar{n}_P = \Lambda g(\nu)\,. \tag{28}$$

Then, defining the total 7S population $\bar{n}_7 \equiv \int n_{7F}(\nu)\,d\nu$, we obtain the relationship ([3]) :

$$\Lambda = \frac{1}{3}\Gamma_{7S}\,\bar{n}_7 + \Gamma_P\,\bar{n}_P \tag{29}$$

which expresses the balance between the numbers of atoms excited to the 7S level (source

([3]) Throughout sections 3 to 6, we make frequent use of the relations

$$\sum_{F'} w_{F'} = \sum_{F'} C_{F'}^{F} = \int f(\nu)\,d\nu = \int g(\nu)\,d\nu = 1\,.$$

term Λ) and of atoms which leave the system, either by $7S \rightarrow 6P_{1/2}$ fluorescence ($\Gamma_{7S}\,\bar{n}_7/3$), or by $6P_{3/2} \rightarrow 6S$ decay ($\Gamma_P\,\bar{n}_P$). We can now calculate the $6P_{3/2}$ population.

Inserting in equation (24) the expression of $n_{7F}(v)$ obtained from equation (28), we obtain an expression for $n_{PF'}(v)$ as a function of $\sum_{F'} n_{PF'}(v)$ and $\bar{n}_P$, which leads to

$$\sum_{F'} n_{PF'}(v) = \frac{\Lambda g(v)\, I(v) + \Gamma^{coll} f(v)\, \bar{n}_P [I(v) + J(v)]}{(\Gamma_P + \Gamma^{coll})\,(1 + I(v))}$$

where

$$I(v) \equiv (\Gamma_P + \Gamma^{coll}) \sum_{F'} \frac{2\, C^F_{F'} + 3\, R^F_{F'}(v)/\Gamma_{7S}}{\mu^F_{F'}\, R^F_{F'}(v) + \Gamma_P + \Gamma^{coll}} \tag{30a}$$

and

$$J(v) \equiv (\Gamma_P + \Gamma^{coll}) \sum_{F'} \frac{w_{F'}}{\mu^F_{F'}\, R^F_{F'}(v) + \Gamma_P + \Gamma^{coll}}\,. \tag{30b}$$

Introducing the dimensionless quantities (functions of the laser frequencies ω_e and ω_d)

$$\mathcal{G} \equiv -2 + 3 \int_{-\infty}^{+\infty} \frac{I(v)}{1 + I(v)}\, g(v)\, dv \tag{31a}$$

$$\mathcal{F} \equiv 2\, \frac{\Gamma^{coll}}{\Gamma_P} \left[1 - \int_{-\infty}^{+\infty} \frac{I(v) + J(v)}{1 + I(v)}\, f(v)\, dv \right], \tag{31b}$$

we obtain the total $6P_{3/2}$ population :

$$\bar{n}_P = \left(\frac{\Lambda}{\Gamma_P} \right) \frac{\mathcal{G} + 2}{3(1 + \mathcal{F}/2)}\,. \tag{32}$$

In the absence of the probe beam, this result is consistent with the zero-order value $\bar{n}_P = \frac{2}{3} \left(\frac{\Lambda}{\Gamma_P} \right)$ since, as we shall see later, $\mathcal{F}$, $\mathcal{G} \propto s$ when $s \rightarrow 0$.

Finally, equations (29) and (32) allow one to calculate the total 7S population, and the fractional increase of the fluorescence intensity caused by the IR laser :

$$\frac{\Delta \mathcal{J}_f(\omega_d)}{\mathcal{J}_f^{(0)}} = \frac{-\mathcal{G} + \mathcal{F}}{1 + \mathcal{F}/2}\,. \tag{33}$$

Let us recall that, if one forgets the two-photon processes, equation (33) is exact for an *unpolarized* probe beam.

We have obtained a very simple form for the fluorescence increase. But the quantities $\mathcal{F}$ and $\mathcal{G}$ are given by rather intricate definitions. A numerical interpretation would not allow an easy physical interpretation. On the contrary, an approximate but analytical expression appears to be very useful.

Approximate expressions for $\mathcal{G}$ *and* $\mathcal{F}$. — The same kind of approximations as for the lowest order calculation (§ 3.1) will be used for the velocity integrals. The sharp function $g(v)$ is replaced by $\delta(v - v_e)$. This remains valid at high saturation (see App. A). Then we have simply

$$\mathcal{G} = -2 + 3\, I(v_e)/(1 + I(v_e))\,.$$

It is useful to separate the ω_d-independent part in $I(\nu_e)$. This leads to :

$$I(\nu_e) = 2 + 3\,s \sum_{F'} C^F_{F'} \frac{1 - 2\,\kappa C^F_{F'}\,\mu^F_{F'}/3}{1 + \Delta^{e2}_{F'} + C^F_{F'}\,\mu^F_{F'}\,\kappa s} \tag{34}$$

where $\Delta^e_{F'} = (\omega_{FF'} - \omega_d + \nu_e)/\gamma$. One finally gets

$$\mathcal{G} = \frac{s \sum_{F'} \mathcal{L}_{F'}(\Delta^e_{F'})}{1 + s \sum_{F'} \mathcal{L}_{F'}(\Delta^e_{F'})}\,, \tag{35}$$

where we have introduced the lorentzian-shaped function :

$$\mathcal{L}_{F'}(x) \equiv C^F_{F'} \frac{1 - 2\,\kappa C^F_{F'}\,\mu^F_{F'}/3}{1 + x^2 + C^F_{F'}\,\mu^F_{F'}\,\kappa s}\,. \tag{36}$$

To obtain an approximate expression for $\mathcal{F}$, we insert equations (30) in equation (31b), and write

$$\mathcal{F} = \frac{2}{3}\,\kappa s \frac{\Gamma^{coll}}{\Gamma_P} \times \int_{-\infty}^{+\infty} \frac{\sum_{F'} \dfrac{C^F_{F'}\,\mu^F_{F'}\,w_{F'}}{1 + \Delta^{\nu 2}_{F'} + C^F_{F'}\,\mu^F_{F'}\,\kappa s}}{1 + \sum_{F''} \dfrac{s C^F_{F''}(1 - (2/3)\,\kappa C^F_{F''}\,\mu^F_{F''})}{1 + \Delta^{\nu 2}_{F''} + C^F_{F''}\,\mu^F_{F''}\,\kappa s}} f(\nu)\,d\nu\,. \tag{37}$$

The integral involves the product of $f(\nu)$, the thermal distribution, by a function corresponding to three resonances of much smaller widths. We note that the saturation broadening of the Lorentz functions (width $2\,\gamma\sqrt{1 + \mu^F_{F'}\,C^F_{F'}\kappa s}$) appears only at strong saturation ($s \gg 1$), since

$$\kappa = \Gamma_{7S}/(\Gamma_P + \Gamma^{coll}) \ll 1\,.$$

In addition, saturation induced overlapping of the Lorentz functions (for $s \gg 1$) makes the denominator in equation (37) nearly constant between the two extreme hfs components. Thus only the high (resp. low) frequency wing of the $F' = F - 1$ (resp. $F' = F + 1$) component brings additional broadening.

We now proceed in the « Doppler limit », that is, supposing that $f(\nu)$ can be taken as constant over the width of a resonance. This approximation is quantitatively valid for low or middle saturations. For strong saturations, it still provides a very useful description of the behaviour of the fluorescence signal. In the Doppler limit, we have

$$\mathcal{F} = \frac{2}{3}\,\kappa s \frac{\Gamma^{coll}}{\Gamma_P} \times \sum_{F'} C^F_{F'}\,\mu^F_{F'}\,w_{F'}\,f(\omega_d - \omega_{FF'}) \int_{-\infty}^{+\infty} \phi_{F'}(\nu)\,d\nu$$

where

$$1/\phi_{F'}(\nu) \simeq \left\{1 + \Delta^{\nu 2}_{F'} + C^F_{F'}\,\mu^F_{F'}\,\kappa s\right\} \times \left\{1 + s\mathcal{L}_{F'}(\Delta^\nu_{F'}) + \sum_{F'' \neq F'} s\mathcal{L}_{F''}(\Delta^\nu_{F'} - \Delta^\nu_{F''})\right\}\,. \tag{38}$$

(We have assumed that the resonances are well resolved.)

Now, remembering that $\int_{-\infty}^{+\infty} dx/(A + Bx^2) = \pi/\sqrt{AB}$, we finally obtain

$$\mathcal{F} = \frac{1}{\mathcal{C}} \left(\frac{\Gamma^{\text{coll}}}{\Gamma_P + \Gamma^{\text{coll}}} \right) \times \frac{2F+1}{32} s \sum_{F'} \frac{C^F_{F'}}{\pi_{F'}} e^{-(\omega_d - \omega_{FF'})^2/2\Omega_D^2} . \quad (39)$$

The weights $\pi_{F'}$, close to 1 at low saturation, embody all saturation effects ; they are given by

$$\pi^2_{F'} = \left\{ 1 + s \sum_{F''} \mathfrak{L}_{F''}(\Delta^{\nu}_{F''} - \Delta^{\nu}_{F'}) \right\} \times \left\{ 1 + s \sum_{F'' \neq F'} \mathfrak{L}_{F''}(\Delta^{\nu}_{F''} - \Delta^{\nu}_{F'}) \right\} (1 + C^F_{F'} \mu^F_{F'} \kappa s) . \quad (40)$$

Interpretation. — The fluorescence increase induced by the probe beam (Eq. (33)) involves the two quantities $\mathcal{G}$ and $\mathcal{F}$, whose respective significances are clear :

i) $\mathcal{G}$ (Eq. (31a)) is related to the sharp function $g(\nu)$ which describes the 7S velocity distribution in the absence of the probe laser (Eq. (8b)). The presence of $\mathcal{G}$ in $\Delta\mathcal{I}_f/\mathcal{I}_f^{(0)}$ describes the decrease of the fluorescence due to the 7S $\rightarrow$ 6P$_{3/2}$ stimulated emission (minus sign in (Eq. (33)).

ii) $\mathcal{F}$ (Eq. (31b)) is related to the thermal distribution $f(\nu)$. Equation (39) shows that $\mathcal{F}$ is proportional to $1/\mathcal{C}$, that is, to the lifetime $1/\Gamma_P$ of the trapped 6P$_{3/2}$ population (Eq. (26c)). The term $\mathcal{F}$ in equation (33) describes the reexcitation of 6P$_{3/2}$ atoms, which results in an increase of the fluorescence.

As opposed to the lowest-order expression (Eq. (27)), the non perturbative solution is not the sum of three independent terms for the three allowed transitions, and this is due to saturation. Saturation takes place in $\mathcal{G}$, in $\mathcal{F}$, and in the denominator $(1 + \mathcal{F}/2)$.

In $\mathcal{G}$, saturation appears in two different manners. From equation (35), when $s\mathfrak{L} \rightarrow \infty$ at strong saturation, then $\mathcal{G} \rightarrow 1$. In this case $-\mathcal{G} = -1$ means that the fluorescence is totally inhibited : stimulated emission has induced all 7S atoms to decay to the 6P$_{3/2}$ level. But stimulated emission cannot be that efficient if the 6P$_{3/2}$ atoms are not quickly quenched or redistributed by collisions. This is the reason of the term $\mu^F_{F'} C^F_{F'} \kappa s$ ($\lesssim \kappa s$) in the denominator of equation (36), which prevents $s\mathfrak{L}$ from taking large values if $\kappa \equiv \Gamma_{7S}/(\Gamma_P + \Gamma^{\text{coll}})$ is not very small compared to unity.

While $\mathcal{G}$ remains always smaller than 1, $\mathcal{F}$ grows to infinity as $s^{1/2}$. Hence from equation (33) the upper limit of the fluorescence increase $\Delta\mathcal{I}_f/\mathcal{I}_f$ is 2 — or more precisely the branching ratio $\Gamma_{\rightarrow 3/2}/\Gamma_{\rightarrow 1/2}$ of the 7S $\rightarrow$ 6P fluorescence. The interpretation is that when the 6P$_{3/2} \rightarrow$ 7S reexcitation rate is high, the only possibility for the atoms to leave the 7S-6P$_{3/2}$ system is the 7S $\rightarrow$ 6P$_{1/2}$ fluorescence, which is then multiplied by a factor $1 + (\Gamma_{\rightarrow 3/2}/\Gamma_{\rightarrow 1/2}) \simeq 3$.

One notes that the term $\mathcal{G}$ in equation (33) is also affected by the denominator $(1 + \mathcal{F}/2)$, which means that the depth of the inhibited fluorescence holes *decreases* at very strong saturation. The trapped 6P$_{3/2}$ atoms can be easily reexcited to the 7S state and this reduces the efficiency of the induced 7S $\rightarrow$ 6P$_{3/2}$ emission when the probe field is saturating. As will be seen in § 3.4 , this behaviour has been observed experimentally, in good agreement with the prediction.

As an example of the results of this calculation, we show a theoretical spectrum for $\Delta\mathcal{I}_f(\omega_d)/\mathcal{I}_f$ obtained from equations (33), (35), (36), (39) and (40) (solid line of Fig. 2). The parameters s, κ, γ, $\mathcal{C}$ have been assigned values corresponding to typical experimental conditions. The dotted line displays the spectrum obtained when the 7S alignment is taken into account by the same method as in section 4.

3.3 PROBE FIELD RESONANT WITH THE UNPOPULATED 7S hfs LEVEL. — We now consider the case of a green laser exciting the 7S, F_e hfs level, and of a detection laser probing the $6P_{3/2}\,F' \leftrightarrow 7S$, F_d transitions, with $F_e \neq F_d$. The hfs splitting in 7S is 2.2 GHz ; so there is no overlap between the two hfs levels. The master equations are similar to equations (23)-(24). The only differences are the following : i) there is no source term for the 7S, F_d population ($\Lambda g(v)$ in Eq. (23) disappears) ; and ii) in the spontaneous $7S \rightarrow 6P$ emission term of equation (24), $\Gamma_{7S}\, C^{F}_{F'}\, n_{7F}(v)$ is replaced by $\{C^{Fe}_{F'}\, \Lambda g(v) + \Gamma_{7S}\, C^{Fd}_{F'}\, n_{7F}(v)\}$.

The method that led to equation (33) now leads to

$$\frac{\Delta \mathfrak{I}_f(\omega_d)}{\mathfrak{I}_f^{(0)}} = \frac{\mathfrak{G}' + \mathcal{F}}{1 + \mathcal{F}/2}$$

where $\mathcal{F}$ is defined as before (Eq. (31b) with F_d replacing F), and

$$\mathfrak{G}' = s \times \frac{\sum_{F'} \frac{2}{3}\, \kappa C^{Fe}_{F'}\, C^{Fd}_{F'}\, \mu^{Fd}_{F'} / \{1 + \Delta^{e2}_{F'} + C^{Fd}_{F'}\, \mu^{Fd}_{F'}\, \kappa s\}}{1 + s \sum_{F'} \mathfrak{L}_{F'}(\Delta^{e}_{F'})}$$

($\Delta^{e}_{F'} \equiv (\omega_{F_d F'} - \omega_d + \nu_e)/\gamma$) replaces equation (35). Instead of the previous three (inhibited fluorescence) holes ($-\,\mathfrak{G}$ in Eq. (33)), the term $+\,\mathfrak{G}'$ now gives rise to *two* positive bumps ($\mathfrak{G}'$ involves the product $C^{Fe}_{F'}\, C^{Fd}_{F'}$ which is zero unless $F' = 3$ or 4). The two bumps indicate the presence, in two of the $6P_{3/2}$ hfs levels coupled to the probe field, of a velocity-selected population resulting from the spontaneous decay of the 7S atoms (Fig. 3a). This velocity-selected population is strongly damped by resonant collisions ; so the two corresponding bumps are expected to be nearly washed off by collisions, except at very low Cs pressure. A typical low pressure spectrum is given in figure 3b.

3.4 COMPARISON WITH EXPERIMENT. — The comparison between theory and experiment has been given in a previous paper [15]. We will recall it briefly here.

Numerous inhibited fluorescence spectra have been recorded at relatively low saturations. All were found in good agreement with the calculated spectra. Only one slight discrepancy has been detected on the wings of the spectra : the calculated fluorescence increase is slightly less than the experimental one (see for instance Fig. 5 in [15]). This is connected with the Doppler limit in the calculation of $\mathcal{F}$.

The agreement remained good in quite different experimental conditions :

i) Excitation selecting a class of atoms of non-zero velocity ($\nu_e \neq 0$ in Eq. (34)). In this case the holes turn out to be shifted by the expected amount with respect to the Doppler profile (Fig. 4 of [15]).

ii) Cs density varied from 5×10^{12} to 6.4×10^{14} at/cm^3. The strong collisional broadening of the 7S-$6P_{3/2}$ coherence does not spoil the agreement between theory and experiment (Fig. 6 of [15]) ; neither does the modification of the trapping of the $6P_{3/2}$ population.

iii) Probe field resonant with the unpopulated level ($F_e \neq F_d$). The experimental spectrum (Fig. 3c) displays the two expected peaks, just like the spectrum calculated in 3.3 (Fig. 3b). We formed the ratios between the heights of the two bumps and the depths of the corresponding inhibited fluorescence holes (when $F_e = F_d$), which are, up to an angular momentum factor, nothing but the ratio $\kappa = \Gamma_{7S}/(\Gamma_P + \Gamma^{coll})$. The low pressure value thus obtained for $\Gamma_P + \Gamma^{coll}$ is close to the $6P_{3/2}$ radiative relaxation rate, as expected when Cs-Cs collisions are negligible.

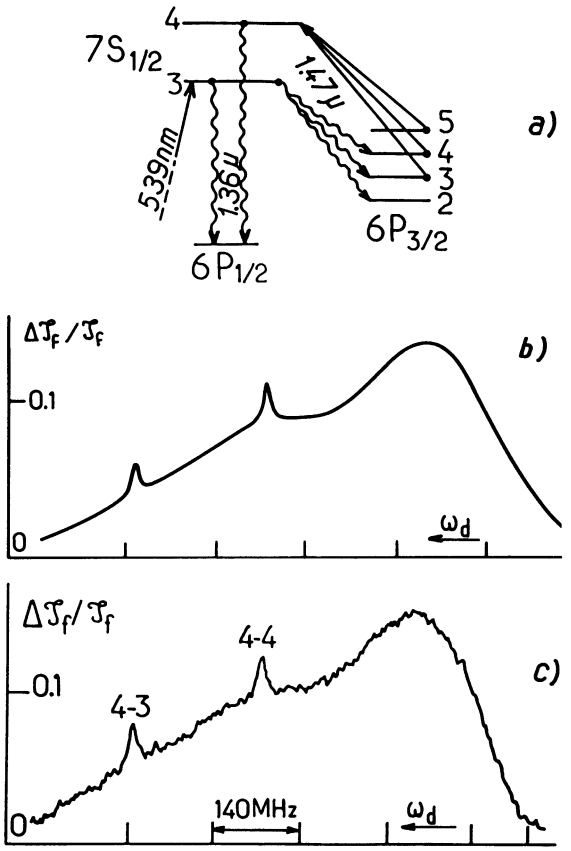

Fig. 3. — Probe laser resonant with the *unpopulated* level a) Level diagram illustrating the case where the green laser excites the 7S, $F = 3$ level while the IR laser probes the 7S, $F = 4 - 6P_{3/2}\,F'$ transitions. b) Theoretical spectrum for the fluorescence increase at low Cs density. c) Experimental spectrum. Cs density 5×10^{12} at/cm^3 ; IR intensity 13 mW/cm^2 ; electric field $E_S = 1\,800$ V/cm.

Having firmly established the quantitative validity of the calculated spectral shape for low or moderate saturation, we also tested the validity at strong saturation. The most salient features predicted for $s \to \infty$ are i) the equality between the maximum value for the fluorescence increase and the branching ratio $\Gamma_{\to 3/2}/\Gamma_{\to 1/2}$ of the 7S fluorescence (theoretical value 1.85 [7]) ; ii) the decrease of the hole depth ; iii) the radiative broadening of the holes.

At first sight the maximum value of $\Delta\mathcal{J}_f/\mathcal{J}_f$ is a very direct measure of the branching ratio. However, the above model assumes the $6P_{3/2}$ and $6P_{1/2}$ levels to be uncoupled. Actually, collisions with ground state atoms induce excitation transfers between them [16]. When the $6P_{3/2}$ level is depopulated by the strongly saturating probe laser, transfer takes place from $6P_{1/2}$ to $6P_{3/2}$. This gives some chance to an atom that has decayed to $6P_{1/2}$ to be cycled once or more. Present lack of information about the transfer cross section at the temperature of our measurements prevents quantitative conclusion. But we believe that this explains why we have observed, at strong saturation, values of $\Delta\mathcal{J}_f/\mathcal{J}_f$ larger than $\Gamma_{\to 3/2}/\Gamma_{\to 1/2}$ (for example $\simeq 2.1$ for $n_{Cs} = 2 \times 10^{14}$ cm^{-3} and $\simeq 2.4$ for $n_{Cs} = 6 \times 10^{14}$ cm^{-3}).

The predicted decrease of the hole depth when $s \to \infty$ has been evidenced owing to a detection procedure particularly sensitive to non-linearities. The probe intensity (and

consequently the saturation) was modulated sinusoidally between zero and a strongly saturating intensity, and the resulting modulation in the fluorescence intensity was detected at the same frequency. Qualitatively, the information obtained this way is the difference between the fluorescence intensities for high and low saturations, i.e. roughly the derivative $d\mathfrak{J}_f/ds$. In the linear regime (modulation amplitude $\delta s \ll 1$), this procedure gives of course the same spectra as the bare fluorescence increase. But as soon as saturation effects become significant, the non-linear s-dependence of the hole depth manifests itself in a reversal of the holes (Fig. 4a). At very large modulation amplitudes, the reversal is such that the holes are turned into sharp peaks (Fig. 4b), indicating that the holes are deeper for $s \simeq 1$ than for $s \gg 1$. The agreement with the corresponding calculated spectra demonstrates the qualitative validity of our theoretical model at strong saturation.

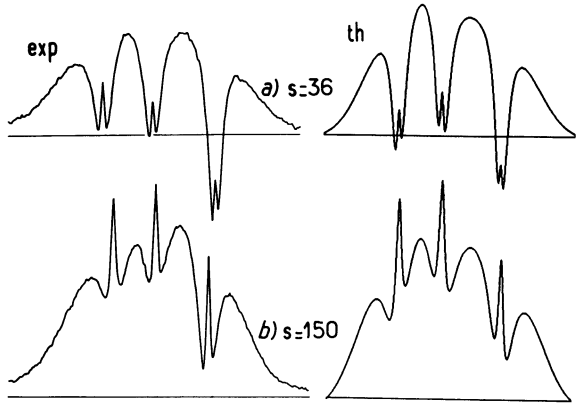

Fig. 4. — Lock-in detection of saturation induced non-linear effects. The *probe intensity* is modulated sinusoidally. The resulting modulation in the fluorescence intensity is plotted as a function of the probe frequency (Cs density 5×10^{12} at/cm^3). The theoretical spectra are obtained by numerical calculation of the integration performed by the lock-in detection.

3.5 QUANTITATIVE RESULTS OBTAINED WITH THE HELP OF THE MODEL. — The most important for us was to study the modification of γ and Γ_P with the cesium density n_{Cs}. This was achieved by fitting, to each experimental record, the theoretical spectrum obtained by adjusting the damping rate γ of the 7S-6P$_{3/2}$ coherence, the lifetime Γ_P of the trapped 6P$_{3/2}$ population, the saturation parameter s, and the detuning ν_e of the excitation laser. This quantitative analysis includes only spectra taken with a non-saturating probe ($s \lesssim 1$).

3.5.1 *Evolution of γ with n_{Cs}.* — The parameter γ plays an important rôle in determining the optimum conditions for the future parity-violation experiment [6]. While the collisional broadening of the resonance lines was known [10, 11], that of the 7S-6P$_{3/2}$ transition was not. Figure 5 shows the plot of γ *versus* n_{Cs} obtained from our measurements. The solid line is a best fit to the experimental points, and gives

$$\gamma/2\pi \text{ (MHz)} = 5.9 + (6.3 \pm 0.7) \times 10^{-14}\, n_{Cs} \text{ (at/cm}^3\text{)}\,, \qquad (41)$$

with a slope uncertainty mainly associated with the Cs density calibration. The collisional broadening of the 7S-6P$_{3/2}$ transition turns out to be slightly less than the corresponding values found in the litterature for the 6S-6P$_{3/2}$ transition : 7.2 [10] and $8.1 \times 10^{-14}\, n_{Cs}$ [11].

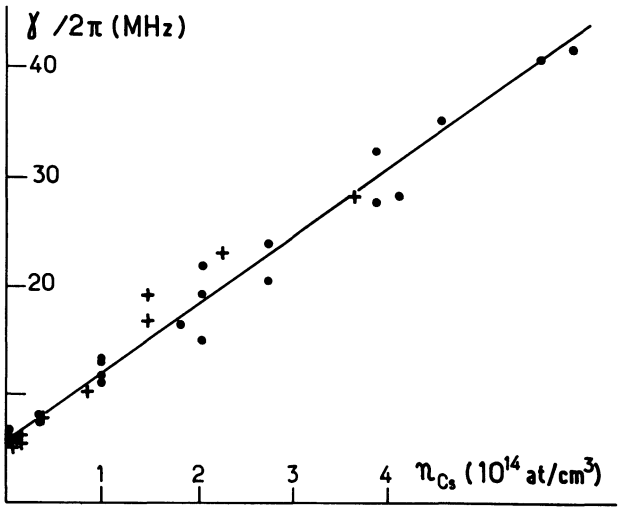

Fig. 5. — Damping rate of the 7S-6P$_{3/2}$ coherence as a function of the Cs density. The dots and crosses were obtained in two different sealed glass cells.

Taking into account the spectral widths of the excitation line and the coherence damping rate of the detection transition, one computes the natural half-width of the holes :

$$\frac{1}{2}\Gamma_{7S} + \frac{1}{2}(\Gamma_{7S} + \Gamma_{6P_{3/2}}) = \left(1/48\ \text{ns} + \frac{1/30\ \text{ns}}{2}\right) = 2\pi \times 4.9\ \text{MHz}\ .$$

The difference with our experimental result (5.9 ± 1 MHz) sets an upper limit of 2 MHz for the instrumental broadening, possible origins of which are : residual frequency jitter of the lasers, residual Doppler width (due to imperfect alignment of the lasers), or traces of a foreign gas in the sealed glass cell.

3.5.2 *Evolution of* Γ_P *with* n_{Cs}. — The height of the observed Doppler profile yields a value for the damping rate Γ_P of the global 6P$_{3/2}$ population. This value was later confirmed by a direct measurement of the time relaxation of the probe beam absorption after a *pulsed* excitation of the forbidden transition.

In figure 6 the obtained values of $\Gamma_P/2\pi$ are plotted as a function of n_{Cs}. One sees

— a rapid decrease when n_{Cs} increases from 5×10^{12} to 5×10^{13} at/cm^3 ;

— a slow increase with n_{Cs} when $n_{Cs} > 10^{14}$ at/cm^3.

At the minimum value $\Gamma_P/2\pi \simeq 30$ kHz the lifetime for the trapped atoms is 100 times larger than the radiative lifetime. As early as 1927, a similar behaviour had been observed by Zemansky for the damping rate of the 6 ^{3}P$_1$ level of mercury which is strongly affected by resonance radiation trapping [17] like the 6P$_{3/2}$ level of cesium. The use of a laser source exciting a forbidden transition allows us to work with a much better defined distribution of excited atoms in space.

The problem of calculating the « trapping factor », i.e. the ratio between the radiative lifetime and the lifetime for the trapped atoms, has been solved by Holstein [13] with certain

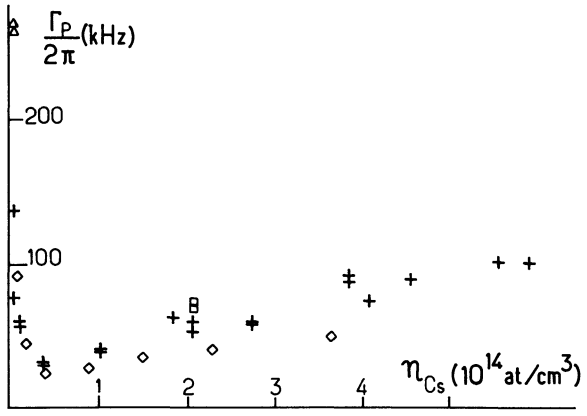

Fig. 6. — Damping rate of the trapped $6P_{3/2}$ population, as a function of the Cs density. Diamonds and crosses were obtained in two different cells, but with the same probe radius 1.4 mm. Triangles and squares were obtained with probe radii of 0.3 and 0.8 mm respectively.

approximations, and has been reconsidered many times [18]. Holstein noticed that, up to a geometrical factor close to unity, the trapping factor is

$$T(d) = \left\{ \int k(\nu)\, e^{-k(\nu)\, d}\, d\nu \right\} \Big/ \int k(\nu)\, d\nu \,,$$

where $k(\nu)$ is the absorption coefficient of the resonance line, and d the smallest dimension of the medium. $T(d)$ is a decreasing function of d, as confirmed by experiments performed with different probe radii. It is worth observing that, since $k(\nu)\, d \gg 1$ at the center of the resonance, $T(d)$ takes its dominant contribution from the wings of the line, where $k(\nu)\, d \simeq 1$. Hence $T(d)$ can be determined by the pressure (homogeneous) broadening, even when the latter is much smaller than the Doppler broadening.

When applied to the atomic level (Cs $6P_{3/2}$) and geometry (cylindrical, defined by the probe beam) relevant here, Holstein's theory predicts for Γ_P at low density a decrease as $1/n_{Cs}$, followed at higher densities by a constant value : $2\pi \times$ 27 kHz for a probe waist of 1.4 mm (more details are given in [19]). This matches the experimental curve (Fig. 6) up to densities of 10^{14} at/cm^3, but does not predict the slow increase at higher densities. A similar increase at high density was observed by Zemansky (Fig. 6 of [17]).

This increase at high density might involve two different collisional processes.

i) Excitation transfer from atom to dimer $Cs^*(6P) + Cs_2 \rightarrow Cs(6S) + Cs_2^*$. A study by Lam *et al.* of the collisional excitation transfer between Na and Na_2 [20] has shown that some of the involved molecular levels can lead to the reverse process and partly restore the excited level's population. Then two different damping rates show up, the smaller one increasing less than quadratically with the atomic density.

ii) Emission of a resonance photon during a collision $Cs^*(6P) + Cs(6S)$. In this case, emission occurs at a wavelength slightly shifted from the resonance [21] and the emitted photon can escape the vapour. An estimate of the resulting contribution to Γ_P indicates a linear increase with the atomic density and a contribution larger than process i) in the pressure range of present interest.

For process ii) the order of magnitude of the corresponding decay rate matches the values of Γ_P observed at high density.

3.6 ZEEMAN SPECTRA. — We have recorded a few Zeeman spectra in a transverse *dc* magnetic field (32 G). Owing to the sharpness of the holes at low Cs density, the Zeeman splittings are resolved. The observed and calculated spectra agree well ([19], Fig. 20). Yet no extensive study has been performed.

4. The helicity-dependent inhibited fluorescence signal.

Investigations of two- and three-level systems driven by two lasers have already demonstrated the sensitivity of sharp spectral structures to the polarizations of the two optical fields. The detection was performed by observing the fluorescence [22] or the transmitted probe beam [23].

In the calculation of sections 2 and 3, we have assumed that all atomic levels involved in the problem had no orientation. We now reconsider the problem when a circularly polarized excitation laser creates a 7S orientation along the probe beam : $p_{7F} \equiv \text{tr}\left\{\rho_{7SF}\,\mathbf{F}\cdot\hat{k}_d\right\} \neq 0$. Then the 7S $\rightarrow$ 6P$_{3/2}$ emission rate, and hence the fluorescence intensity, are functions of the product $\xi_d\, p_{7F}$, where $\xi_d \equiv \Im\text{m}\,[\hat{k}_d \cdot (\hat{\varepsilon}_d^* \wedge \hat{\varepsilon}_d)]$ is the probe beam helicity. Modulation of ξ_d and synchronous detection of the fluorescence thus offers a new possibility of measuring the 7S orientation, *without fluorescence polarization analysis*. This is interesting since the statistical accuracy of the ENS parity-violation measurement had up to now been ultimately limited by the need of analysing the polarization of the fluorescence [24].

In order to test the possible advantages of this new method of detecting orientation, we have recorded spectra while modulating the helicities ξ_e and ξ_d of the excitation and detection beams, and detecting the cross-modulated $\xi_e\,\xi_d$ contribution in the fluorescence. The linear polarizations were also modulated, at the same frequencies as the helicities, but in phase quadrature with them. This generates no spurious $\xi_e\,\xi_d$-type modulation, as proved by the absence of signal when only the linear polarizations are modulated.

This section is devoted to the calculation of the theoretical spectrum, and to its use in exploiting the experimental data. A constant rule is applied throughout this section : in the density matrix, we omit all terms that do not contribute to the signal of interest, i.e. to a 7S population having the $\xi_e\,\xi_d$ signature.

4.1 LOWEST-ORDER CALCULATION. — In absence of the probe beam, the contribution proportional to ξ_e in the 7S density matrix is expressed as :

$$\rho_{7F}^{(0)}(\nu) = +\,\xi_e \Lambda^{(1)} \frac{3\,\mathbf{F}\cdot\hat{k}}{F(F+1)} \frac{\mathbb{P}(7SF)}{2F+1}\,. \tag{42}$$

The expression for the orientation source term $\Lambda^{(1)}$ is given in [19]. Here $\Lambda^{(1)}$ can be considered as an overall normalization constant. We now insert equation (42) in equation (14) and obtain the first order contribution

$$n_{7F}^{(1)}(\nu) = -\frac{1}{\Gamma_{7S}} \sum_{F'} \frac{(2/\gamma)\,|\mathcal{E}_d/2\,\hbar|^2}{1+\Delta_{F'}^2} \times \text{tr}\;\left\{\mathfrak{D}_{FF'}\,\mathfrak{D}_{FF'}^{\dagger}\,\rho_{7F}^{(0)}(\nu)\right\}\,.$$

We have omitted the 6P$_{3/2}$ contribution because i) at lowest order, the 6P$_{3/2}$ population is not modulated as ξ_e ; ii) the 6P$_{3/2}$ orientation brought by spontaneous decay is destroyed by collisions, as shown by experiments. We calculate the trace using equation (20) ; we then obtain three contributions, only the second of which is non-zero (helpful trace formulae are

given in [19], App. C). Finally the $\xi_e\,\xi_d$-modulated contribution in the integrated 7S population is written as

$$\bar{n}_7^{(1)} = -\,\xi_e\,\xi_d\,\frac{\Lambda^{(1)}}{2F(F+1)/3}\sum_{F'}\frac{sC^{F}_{F'}\,a\,\begin{matrix}F\\\downarrow\\F'\end{matrix}}{1+\Delta^{e2}_{F'}}\,. \tag{43}$$

The integration has been performed using approximation (25a). Unlike the population signal (Eq. (27)), the lowest-order calculation of the orientation signal has no Doppler broadened contribution.

When compared to experimental spectra recorded at a saturation level $s \simeq 1$, the lowest order spectral shape turns out to predict the respective signs of the three hfs components and the order of magnitude of the signal, but fails to predict the ratios of the components, with discrepancies up to a factor 2.

In fact the orientation signal is more heavily affected by saturation than the population signal previously calculated. The reason is that, in addition to the saturation of the populations, that affects both signals, the orientation signal also reflects the effects of saturation acting upon the 7S orientation. This signal thus requires a more complete treatment of the saturation effects, which is now to be presented.

4.2 NON-PERTURBATIVE TREATMENT INCLUDING ALIGNMENT. — In this section we present the starting points and the results of the more complete treatment and we discuss its validity. Technical details are deferred to appendix C.

4.2.1 *Assumptions.* — Three assumptions are made. We assume that :

i) in the $6P_{3/2}$ resonance level, orientation and alignment are completely washed off by resonant collisions.

ii) The density matrix can be expanded in powers of $F_k \equiv \mathbf{F}\cdot\hat{k}$ ($\hat{k}$ is the unit vector along the direction of the beams) because the system is invariant in any rotation around the direction of the two circularly polarized beams.

iii) Tensors of order higher than 2 are negligible. The validity of these assumptions is checked in § 4.2.3.

We now write the density matrix in terms of populations in the 7SF and $6P_{3/2}$ levels, of orientation ($p_{7F}(\nu)$) and alignment ($q_{7F}(\nu)$) along $\hat{k}$ in the 7SF level :

$$p_{7F}(\nu) \equiv \mathrm{tr}\,\left\{\rho_{7F}(\nu)\,\mathbf{F}\cdot\hat{k}\right\} \tag{44}$$

$$q_{7F}(\nu) \equiv \mathrm{tr}\,\left\{\rho_{7F}(\nu)\left[1-\frac{(\mathbf{F}\cdot\hat{k})^2}{F(F+1)/3}\right]\right\}\,. \tag{45}$$

Next we neglect the effect of Cs(6S)-Cs(7S) collisions on the orientation and alignment as we already did for the populations. From previous Hanle effect measurements, we know that this effect is small at our operating densities [12]. Then $n_{7F}(\nu)$, $p_{7F}(\nu)$, $q_{7F}(\nu)$, and $n_{PF'}(\nu)$ obey the steady-state equations written in appendix C (Eqs. (C.1)). From these we deduce the relation :

$$(\Gamma_{7S}/3)\,\bar{n}_7 + \Gamma_P\,\bar{n}_P = 0 \tag{46}$$

which reflects the absence of any population source with $\xi_e\,\xi_d$ dependence (compare with Eq. (29)).

4.2.2 *Results.* — There is no basic difference between the new steady-state equations and equations (23)-(24) ; so the calculation follows the same method (see App. C). The solution reads :

$$\bar{n}_7 = \xi_d \, \xi_e \left(\frac{\Lambda^{(1)}}{\Gamma_{7S}} \right) \frac{-\mathfrak{G}_\xi}{1 + \mathcal{F}_\xi/2} \cdot \tag{47}$$

Exact definitions of $\mathfrak{G}_\xi$ and $\mathcal{F}_\xi$ are given by equations (C.4). At low saturation, the plot of $\mathfrak{G}_\xi$ *versus* ω_d is composed of three resolved Lorentz-shaped resonances. The quantity $\mathcal{F}_\xi$ is a Doppler-broadened function similar to $\mathcal{F}$. It only affects the heights of the resonances when saturation effects cannot be neglected.

In appendix C, the notations adopted to write $\mathcal{F}_\xi$ and $\mathfrak{G}_\xi$ aim at emphasizing the corrections introduced by taking the alignment into account. For $s = 1$, these corrections affect the value of $\bar{n}_7$ by 1.5 to 13.5 %, depending on the hfs component. We also give approximate analytical expressions of $\mathfrak{G}_\xi$ and $\mathcal{F}_\xi$, by using the same kind of arguments as in § 3.2.

4.2.3 *Validity of the solution.* — We have performed an approximate, analytical treatment that aims at providing a quantitative theoretical basis to interpret and exploit helicity-dependent spectra recorded with saturations up to $s \simeq 1$. We now discuss the accuracy of the solution obtained in this way.

i) We have assumed that the 6P$_{3/2}$ orientation and alignment, strongly damped by collisions, can be omitted. The validity of this assumption is evidenced by probing the transitions between the 6P$_{3/2}$ F' levels and the 7S hyperfine level not populated (and not oriented) by the excitation laser. In this way we detect only the 6P$_{3/2}$ orientation. The spectra then turn out to be always consistent with mere noise, even at strong saturation. Thus the 6P$_{3/2}$ orientation, too small to be detected, cannot give any contribution to the signal.

ii) We have restricted the 7S density matrix to the irreducible tensors of rank 0, 1, and 2. The contribution of the omitted higher order tensors cannot be isolated as in i). However the 7S atoms are prepared with tensors of orders 0 and 1 and one interaction with the probe beam couples the tensors of order K with those of orders K, $K \pm 1$, and $K \pm 2$. Consequently one easily convinces oneself that the omission of the tensor of order K in the 7SF density matrix has no consequence before the s^K-term in the perturbative development. Recalling that the parameter of the expansion is not s but $sC^F_{F'}$ (and that $C^F_{F'}$ lies between 0.1 and 0.6), we expect the corrections for the omitted terms of order 3 to be smaller than the aligment induced corrections, i.e. smaller than $\simeq 10$ %. Actually, explicit evaluation of this correction yields 5 % for $s = 1$. So we believe that, up to $s = 1$, our solution is correct to better than 10 %.

4.3 COMPARISON WITH EXPERIMENTAL LOW SATURATION SPECTRA. — Figure 7 displays experimental spectra recorded with a saturation s close to 1. The lower curves are a theoretical fit and reproduce the spectra satisfactorily. That our non-perturbative model correctly describes the saturation effects, is more easily seen in figure 8, where we have plotted the heights of the six hfs components as a function of the saturation parameter. A lowest order treatment would completely fail as soon as $s \gtrsim 0.4$. Two theoretical curves are displayed. The solid curve have been calculated with the value $\Gamma_P/2\pi = 100$ kHz obtained from the inhibited fluorescence spectra recorded in the same conditions. For $s \gtrsim 0.4$ a value $\simeq 75$ kHz (dashed curve) gives a better agreement, especially on the $F = 4 \rightarrow F' = 5$ component, which is the most affected by saturation.

A certain difference in the spatial distribution of the atoms probed in the inhibited fluorescence and helicity-dependent spectra may be the reason for this tendency of the two kinds of spectra to lead to slightly different values of Γ_P. We have not tried to account for this

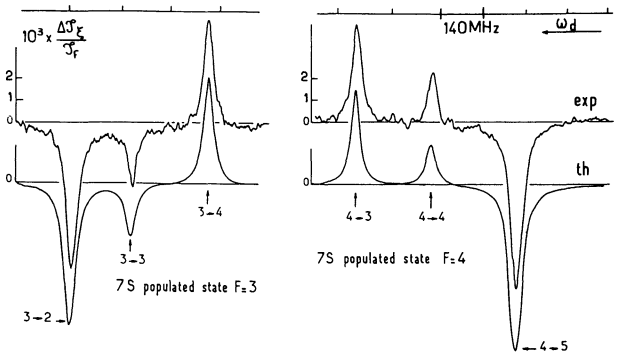

Fig. 7. — Helicity-dependent spectra. Excitation and detection helicities are modulated. The amplitude $\Delta \mathcal{J}_\xi$ of the resulting cross-modulation in the fluorescence intensity, normalized to the bare fluorescence intensity $\mathcal{J}_f^{(0)}$, is plotted *vs.* the probe frequency. Cs density 10^{14} at/cm^3 ; electric field E_S = 1 000 V/cm ; probe intensity 17 mW/cm^2. The theoretical spectra are calculated with $s = 1.2$ and $\gamma/2\pi$ = 12 MHz.

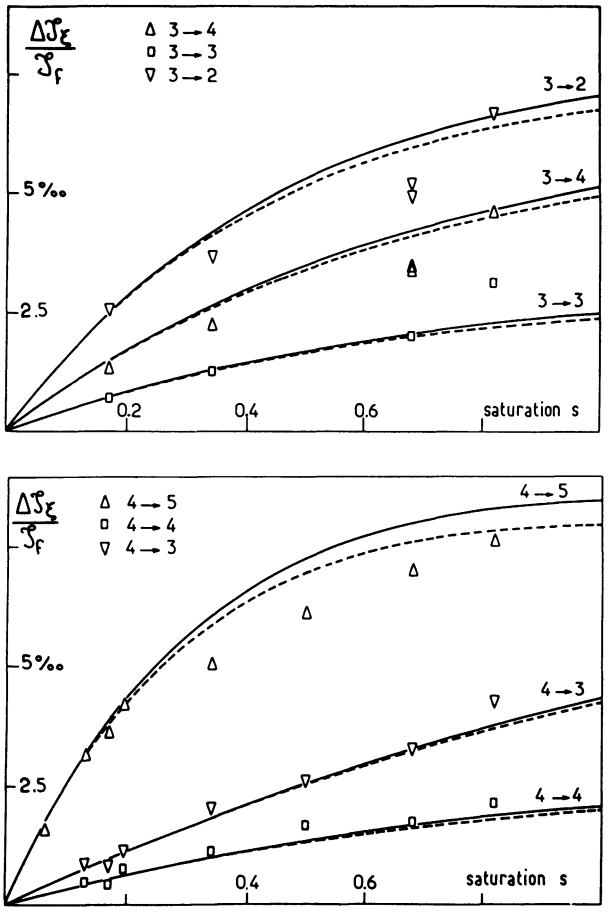

Fig. 8. — Heights of the six hfs components of the helicity-dependent signal *versus* saturation parameter s. Experimental points : $n_{Cs} = 2 \times 10^{14}$ at/cm^3. Theoretical curves are obtained for $\gamma/2\pi$ = 18 MHz, $\Gamma_P/2\pi$ = 100 kHz (solid line) and 75 kHz (dashed line).

effect. In fact, the important point for us is that the two values of Γ_P lead to the same optimized overall normalization of the spectra. The latter yields the orientation source term $\Lambda^{(1)}$.

4.4 QUANTITATIVE RESULTS.

4.4.1 *Dependence of the* 7S-6P$_{3/2}$ *damping rate on the* Cs *density.* — A value of γ can be obtained from the fit of the $\xi_e \xi_d$-dependent spectra. Five measurements have been performed from 0.8 to 20 mtorr (Fig. 9). The resulting linear law

$$\gamma/2\pi \text{ (MHz)} = 4.9 + (6.5 \pm 0.7) \times 10^{-14} n_{Cs} \text{ (at/cm}^3\text{)}$$

is in good agreement with equation (41), obtained from the inhibited fluorescence spectra.

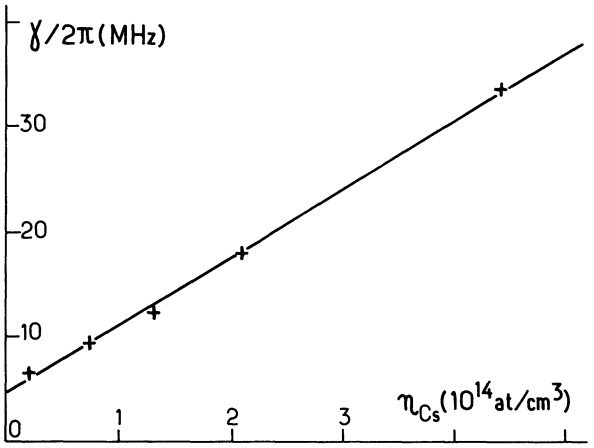

Fig. 9. — Damping rate of the 7S-6P$_{3/2}$ coherence *versus* Cs density as extracted from the helicity-dependent spectra, and linear fit.

4.4.2 *Determination of the vector-to-scalar polarizability ratio.* — The angular momentum transfer from the (circular) photons to the 7S atoms operates through spin-orbit coupling. As a result, the orientation source term $\Lambda^{(1)}$ differs from the population source term Λ by a factor which, up to a known angular momentum factor, is nothing but the vector-to-scalar polarizability ratio β/α of the 6S-7S transition. This ratio has been measured to a precision of one percent : $\alpha/\beta = -9.9 \pm 0.1$ [25].

From the value of $\Lambda^{(1)}$ that optimizes the fit of figure 8, we have deduced $|\alpha/\beta| = 10$ ($\pm$ 15 %), which agrees with the previous measurements. The uncertainty accounts for the noise on the experimental data and for the uncertainty in the saturation parameter as well as in the theory.

A strong motivation for this study was its possible natural extension to a measurement of a parity-violating 7S orientation ([4]) using detection of the 7S-6P fluorescence. In *the ratio* of the

([4]) The PV orientation in 7S results from interference between the PV and Stark-induced E_1 amplitudes in the 6S-7S excitation. It is created in a direction normal to the excitation beam. By Hanle effect in a suitable magnetic field, it acquires a component along the beam. It can be probed like the parity-conserving orientation, and discriminated owing to a different behaviour under reversal of E and H.

PV orientation to the orientation detected here (accurately known from previous measurements of β/α) the accuracy would be mainly limited by noise. In the measurements presented here, the measuring time was short ($\simeq$ 10 s). Moreover, since the use of a probe beam makes fluorescence polarization analysis unnecessary, one can expect better collection efficiencies than in the previous parity violation measurement performed in our laboratory [24]. Which sensitivity can ultimately be attained, becomes a matter of ingenuity in designing an optical detection system best suited to this new scheme.

4.5 THE ξ-DEPENDENT SIGNAL AT STRONG SATURATION. — As usual, saturation broadens the resonances. But while the low saturation spectra are formed by three Lorentz-shaped resonances, at strong saturation a new feature appears (Fig. 10). The $F \rightarrow F' = F + 1$ components undergo a self-reversal, while the others do not. For $s = 60$, the signal is close to zero at the center of the $4 \rightarrow 5$ resonance.

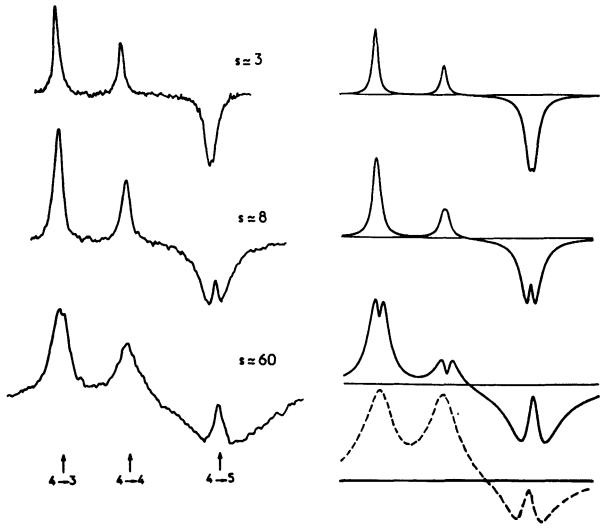

Fig. 10. — Evolution of the helicity-dependent spectra with the saturation parameter. Cs density 2×10^{13} at/cm^3 ; electric field E_S = 2 000 V/cm. The theoretical spectra are calculated for the nuclear spin $I = 7/2$, except the dashed one which is calculated for $I = 3/2$.

In section 3, we saw that our model remains qualitatively predictive at strong saturation, though some of the approximations then become unjustified. One may now wonder whether the calculated ξ-dependent signal can be extrapolated to saturations much greater than the saturations $s \lesssim 1$ for which it was built. The theoretical spectra of figure 10 show that the agreement with experiment remains fairly good, at least qualitatively, up to $s \simeq 8$. For $s \simeq 60$ however, the model fails to reproduce the behaviour difference between the $F \rightarrow F' = F + 1$ component and the other components : it predicts that all resonances are more or less reversed, which is not confirmed by experiment.

As will be shown now, the specific behaviour of the $F \rightarrow F' = F + 1$ component takes it origin in the way the Zeeman sublevels of the (oriented) 7SF level are coupled to the $6P_{3/2}$ F' sublevels by the circularly polarized probe beam.

When $F' = F + 1$, *all* 7S,Fm sublevels are coupled by the probe laser, whatever the probe helicity. If the probe beam is strongly saturating, its effect is the same on all 7S,Fm sublevels :

it equalizes the populations. So the 7S population is the same for a probe beam of helicity $\xi_d = -1$ or $+1$. There is no signal associated with the reversal of ξ_d. This explains why the ξ-dependent signal goes down to zero at the center of the $F \rightarrow F' = F + 1$ resonances for strong saturation.

The conclusion is different if one considers a $F \rightarrow F' = F$ component : then there is one unpaired sublevel ($m = \xi_d F$) which is *unaffected by the probe beam.* Since the 7SF level is oriented by the excitation laser, the populations of the $m = +F$ and $m = -F$ states are different. Therefore the reversal of ξ_d necessarily gives rise to a non-zero signal, even at strong saturation. The same argument holds when $F' = F - 1$, in which case two Zeeman sublevels ($m = \xi_d F$ and $\xi_d(F-1)$) remain unpaired.

So we understand the physical origin of the different behaviour of the $F' = F + 1$ components. And we also understand that the model, which omits the higher-order tensors, cannot account for the specific effect of one or two sublevels. When applied to the $F = 1 \rightarrow F' = 0, 1, 2$ transitions of an alkali of $I = 3/2$, the model should be correct since it accounts for all tensors (population, orientation, alignment) in an $F = 1$ level. The corresponding theoretical spectrum (dashed line of Fig. 10) shows the expected features : only the $1 \rightarrow 2$ component is reversed.

5. Calculation of the transmitted probe beam.

In some of the experiments we also observed the intensity and polarization of the transmitted probe beam [26]. The helicity of the excitation beam, is modulated as before. The polarization of the probe beam is now linear and fixed. We now consider that the excited vapour gives rise, at the wavelength of the probe transition, to amplification, circular dichroism, and optical rotation. These are calculated using the semi-classical, steady-state propagation equation

$$\frac{\partial}{\partial z}\,\mathcal{E}_d(z) = \frac{i\,\omega_d}{2\,\varepsilon_0\,c}\,\langle \mathfrak{D} \rangle\,(z)\,. \tag{48}$$

This equation relates the amplitude of the probe electric field, defined so that the electric field is given by

$$\mathcal{E}_d(z,t) = \frac{1}{2}\,\mathcal{E}_d(z) \times \exp\{-i\,\omega_d(t - z/c)\} + \text{c.c.}\,,$$

to the amplitude of the macroscopic polarization of the vapour, defined so that the macroscopic polarization is

$$\langle \mathfrak{D} \rangle\,(z,t) = \frac{1}{2}\,\langle \mathfrak{D} \rangle\,(z) \exp\{-i\,\omega_d(t - z/c)\} + \text{c.c.}$$

We can assume that $\langle \mathfrak{D} \rangle\,(z)$ does not depend on z since the fractional intensity change never reaches one percent for the probe beam, and is even much smaller for the excitation beam. The macroscopic dipole is obtained from velocity integration :

$$\langle \mathfrak{D} \rangle = 2 \int \sum_{F'} \text{tr}\,\{\rho_{FF'}(v)\,\mathfrak{D}\}\; e^{i(\omega_d - \omega_{FF'} - v)t}\,dv$$

(the notations are the same as in the previous sections).

5.1 THE AMPLIFICATION SPECTRUM. — We shall see that the probe amplification is related to the fluorescence increase. Multiplying both sides of equation (48) by $\mathcal{E}_d^*(z)$, one finds

$$\frac{\partial}{\partial z} |\mathcal{E}_d(z)|^2 = \frac{\omega_d}{\varepsilon_0 c} \int i\mathcal{E}_d^*(z) \times \sum_{F'} e^{i(\omega_d - \omega_{FF'} - \nu)t} \operatorname{tr} \{\rho_{FF'}(\nu)\, \mathfrak{D}_{FF'}^\dagger\}\, d\nu + \text{c.c.}$$

Then, using equation (11) and $\dot{n}_{7F} = 0$, one easily derives the equation

$$\frac{1}{\hbar\omega_d} \frac{\partial}{\partial z} \frac{\varepsilon_0 c}{2} \times |\mathcal{E}_d(z)|^2 + \Gamma_{7S}\, \bar{n}_{7F} = \Lambda = \Gamma_{7S}\, \bar{n}_{7F^{(0)}}$$

which expresses the conservation of the total number of (induced or spontaneous) emitted photons. In other words, amplification occurs at the expense of a fluorescence decrease. Finally, in the low absorption limit valid here, we relate the fractional intensity change at the probe wavelength to the fluorescence increase

$$\frac{\Delta I}{I} = \ell \frac{\Lambda}{\Gamma_{7S}} \left\{ \frac{4\pi}{137} \frac{\omega_d}{\gamma} \frac{|\langle 7S_{1/2} \| \mathbf{r} \| 6P_{3/2} \rangle|^2}{6} \right\} \times \left(-\frac{1}{s} \frac{\Delta \mathfrak{I}_f}{\mathfrak{I}_f} \right). \tag{49}$$

The two beams are supposed to have the same dimensions. ℓ is the length of the excited vapour, and 1/137 represents the fine structure constant. The factor in curly braces is easily recognized as the induced emission cross section on the $7S \rightarrow 6P_{3/2}$ transition. The proportionality of $\Delta I/I$ to $\Delta\mathfrak{I}_f/\mathfrak{I}_f$ has been evidenced by simultaneous recording of the fluorescence intensity and the transmission of the probe beam (Fig. 11). The proportionality, including the minus sign in equation (49), is quite conspicuous.

5.2 MODIFICATION OF THE PROBE BEAM POLARIZATION. — Let us denote $\hat{\varepsilon}_d$ the (linear) polarization of the incoming probe beam, and write $\mathcal{E}_d(0) = \mathcal{E}_d(0)\, \hat{\varepsilon}_d$. Passing through the oriented vapour, the probe beam acquires a component along the perpendicular polarization $\hat{\varepsilon}_\perp \equiv \hat{k}_d \wedge \hat{\varepsilon}_d$, and we write

$$\mathcal{E}_d(\ell) = \mathcal{E}_d(\ell)\, \hat{\varepsilon}_d + \mathcal{E}_\perp(\ell)\, \hat{\varepsilon}_\perp .$$

Since the optical density is small we have

$$\mathcal{E}_\perp(\ell) = \frac{i\omega_d \ell}{\varepsilon_0 c} \times \int \sum_{F'} e^{i(\omega_d - \omega_{FF'} - \nu)t} \operatorname{tr} \{\rho_{FF'}(\nu)\, \mathfrak{D} \cdot \hat{\varepsilon}_\perp\}\, d\nu .$$

We use equation (13) and express $\mathcal{E}_\perp(\ell)$ in terms of $\mathcal{E}_d(0)$ and the density matrices in the 7SF and $6P_{3/2}$ F′ levels. We shall neglect the $6P_{3/2}$ contribution since i) we know that orientation or alignment do not survive in the $6P_{3/2}$ level (see § 4.2.3.i) ; and ii) as shown below, a population cannot contribute to $\mathcal{E}_\perp$. We use the operator $\vec{\mathfrak{C}}$ (App. B), to write

$$\mathcal{E}_\perp(\ell) = \frac{\mathcal{E}_d(0)\, \omega_d \ell}{2\hbar\varepsilon_0 c} \times \int \sum_{F'} \frac{\operatorname{tr} \left\{ \hat{\varepsilon}_d \cdot \vec{\mathfrak{C}} \begin{matrix} F \\ \downarrow \\ F' \end{matrix} \cdot \hat{\varepsilon}_\perp\, \rho_{7F}(\nu) \right\}}{i(\omega_{FF'} - \omega_d + \nu) + \gamma}\, d\nu . \tag{50}$$

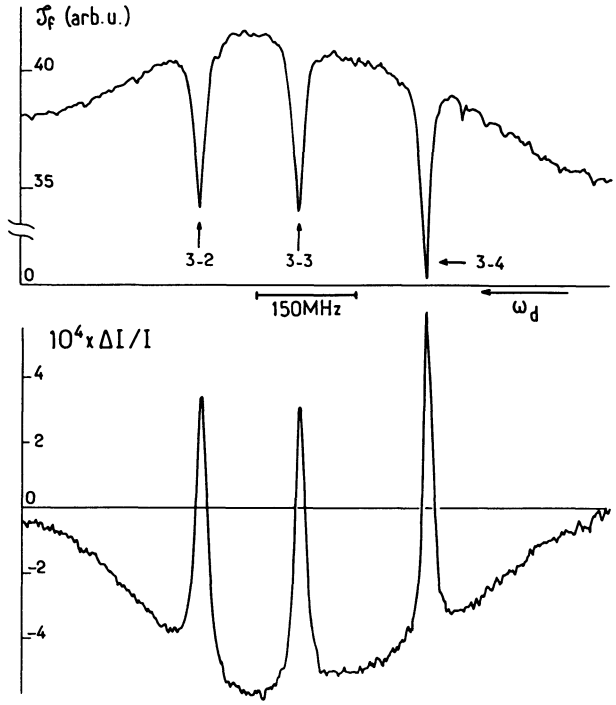

Fig. 11. — Simultaneous recording of the fluorescence intensity (upper curve) and of the probe amplification (lower curve). The green laser excites the 7S, $F = 3$ level. The probe frequency is swept over the 7S, $F = 3 \rightarrow 6P_{3/2}\,F'$ resonances. Cs density 3×10^{13} at/cm^3 ; electric field 2 000 V/cm. The fluorescence intensity baseline is slightly affected by a slow intensity drift of the excitation laser.

From equations (18) and (B.7), and with the definitions $\hat{\varepsilon}_{1(2)} \equiv \hat{\varepsilon}_d + (-)\,\hat{\varepsilon}_\perp$, we obtain

$$\hat{\varepsilon}_d \cdot \vec{\vec{\mathcal{C}}} \underset{F'}{\overset{F}{\downarrow}} \cdot \hat{\varepsilon}_\perp = \frac{|\langle 7S_{1/2} \| \mathfrak{D} \| 6P_{3/2} \rangle|^2}{F(F+1)} \frac{C^F_{F'}}{2} \times \left\{ \frac{i}{2} a \underset{F'}{\overset{F}{\downarrow}} \mathbf{F} \cdot \hat{k} + b \underset{F'}{\overset{F}{\downarrow}} \frac{(\mathbf{F} \cdot \hat{\varepsilon}_1)^2 - (\mathbf{F} \cdot \hat{\varepsilon}_2)^2}{4} \right\} .$$

This operator contains only tensors of orders 1 and 2. So, only an orientation (along $\hat{k}$), or an alignment (with axes at $\pm 45°$ with respect to $\hat{\varepsilon}_d$) can contribute to $\mathfrak{E}_\perp$. In the present case, none of the lasers can create such an alignment. We only have to take into account the 7S orientation

$$p_{7F}(\nu) \equiv \mathrm{tr}\,\{\rho_{7F}(\nu)\mathbf{F} \cdot \hat{k}\} .$$

As in section 3, we have to solve the steady-state equations for the density matrix. But a great difference arises from the fact that the probe beam interacting with the Cs atoms is now polarized *linearly*. As a result the orientation is not coupled to the population. Omitting the tensors of rank $\geqslant 3$, the steady-state orientation now obeys the equation

$$0 = -\Gamma_{7S}\, p_{7F}(\nu) + \xi_e\, \Lambda^{(1)} g(\nu) - \sum_{F'} \lambda_{11}\, R^F_{F'}(\nu)\, p_{7F}(\nu)$$

(the coefficients λ_{ij} are defined in App. C). The expression for p_{7F} is then easily obtained.

Once inserted in equation (50) it gives $\mathcal{E}_\perp$. The result is more conveniently expressed in terms of a difference between the refractive indices n_+ and n_- for photons of respective helicities $\xi_d = +1$ and -1. Then $\mathcal{E}_\perp = \mathcal{E}_d(n_- - n_+)\,\ell\,\omega_d/2c$, and

$$\frac{n_- - n_+}{2} = -\xi_e A^{(1)} \frac{2\pi c\,|\langle 7S_{1/2}\|\mathbf{r}\|6P_{3/2}\rangle|^2}{137 \times 6\,\gamma\Gamma_{7S}} \times \frac{\sum_{F'} \lambda_{01} C^F_{F'} \left(\dfrac{\Delta^e_{F'} + i}{1 + \Delta^{e2}_{F'}} \right)}{1 + \sum_{F'} \dfrac{\lambda_{11}\, s C^F_{F'}}{1 + \Delta^{e2}_{F'}}} \tag{51}$$

(the integration has been approximated, as previously, using Eq. (25a)).

As expected, the circular dichroism spectrum (imaginary part of $n_+ - n_-$) has a dispersion shape. But now, despite saturation effects, the spectral shape remains fairly simple, much simpler than the helicity-dependent signal observed by fluorescence (App. C).

Comparison with experiment. — Figure 12a illustrates the agreement between theory and experiment on the optical rotation signal. As expected from equation (51), no Doppler-broadened signal can be observed. The excellent S/N ratio allows accurate comparison between theory and experiment. The agreement is good, despite large saturation effects : a lowest order solution, which predicts heights 69 % higher for the $4 \rightarrow 5$ resonance and $\simeq 15$ % higher for the $4 \rightarrow 4$ and $4 \rightarrow 3$ resonances, would fail to reproduce the experimental spectra. Circular dichroism spectra also lead to a good agreement (Fig. 12b). As in the case of the helicity-dependent spectra of section 4, the overall normalization of the spectra leads to the correct value $|\alpha/\beta| \simeq 10$ of the scalar-to-vector polarizability ratio of the forbidden transition.

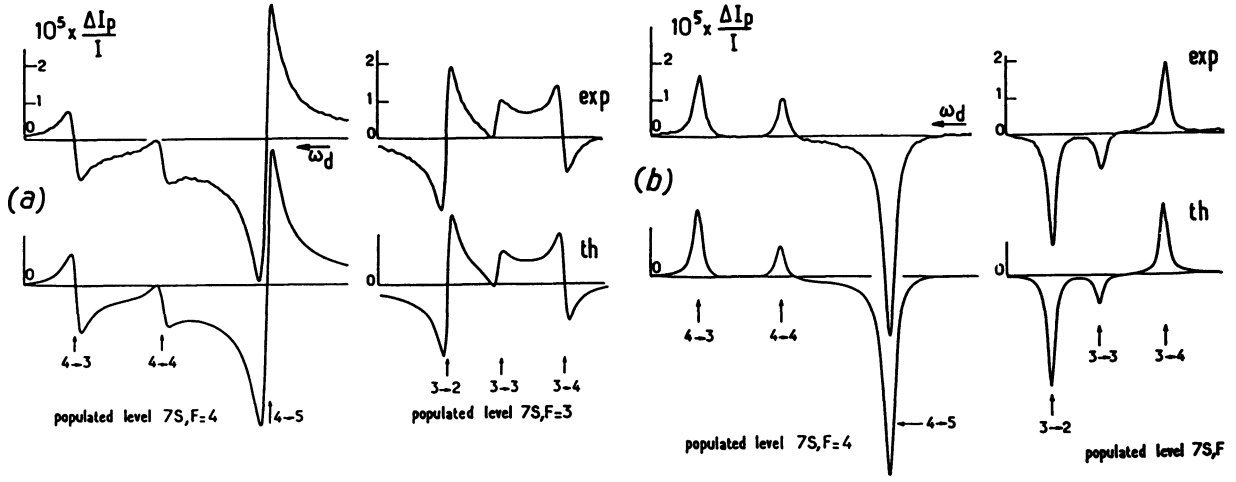

Fig. 12. — Transmitted probe beam analysis. The probe intensity is detected behind an analyzer nearly crossed with the incoming probe polarization (uncrossing angle 7.5×10^{-2} radian). The excitation helicity ξ_e is modulated. The amplitude of the resulting modulation is plotted *versus* the probe frequency. a) Optical rotation spectra ; b) circular dichroism spectra (a quarter-wave plate is inserted before the analyzer). Cs density 10^{14} at/cm^3 ; electric field 2 000 V/cm. Theoretical spectra for $s = 1$, and $\gamma/2\pi = 12$ MHz.

6. Conclusion.

In this paper we have presented a theoretical approach to the Cs 6S-7S-6P$_{3/2}$ forbidden three-level system, and illustrated the agreement with experiment. We have chosen an approximate but analytical resolution of the master equations. This was possible owing to the highly forbidden character of the transition used to excite the Cs atoms. Several approximations were therefore justified : the excitation has been treated at the lowest order ; the coherent 6S-6P$_{3/2}$ process has been neglected as compared to the stepwise 6S→7S→6P$_{3/2}$ process, which largely dominates ; the hierarchy between the width of the forbidden transition, the width of the 7S-6P$_{3/2}$ transition and the Doppler width, has allowed simplified integration over the velocities. Finally, omitting tensor orders $\gtrsim 3$, we have achieved a non-perturbative resolution, quantitatively valid up to values $s \simeq 1$ for the saturation parameter. Only in strongly saturating laser fields, in the case of fluorescence spectra characteristic of the 7S orientation, and only for the $\Delta F = 0$ and -1 transitions, does the omission of the higher order tensors lead to a conspicuous difference between calculated and observed spectra. At moderate or low saturation the calculated and experimental spectra show good agreement. Theoretical fits of the data have yielded numerical values of several parameters of the forbidden system, such as the damping rate of the 7S-6P$_{3/2}$ coherence.

The 7S orientation has been measured by detection of the 7S → 6P fluorescence without polarization analysis, and by detection of the transmitted probe polarization as well. The first technique appears interesting since it could help to improve the detection efficiency of the method used in our laboratory for previous parity violation measurements. Yet the second method appears to be more promising : observation of the transmitted probe beam allows one to detect almost *all* excited atoms. With the PV orientation (or alignment) in the excited level is associated to a circular (or linear) dichroism for both the excitation and probe beams. But the optical density for the probe can be much greater since it is proportional to the density of excited atoms and to the induced emission cross section. The fractional intensity change $\Delta I/I$ can even reach or exceed 1 after a *pulsed* excitation of the forbidden transition. In this case the photon noise associated with the probe beam will no longer dominate the noise associated with the atomic signal itself. In addition, when $\Delta I/I > 1$, the propagation through the vapour can lead to an amplification of the left-right asymmetry [6]. These attractive features have led us to an experimental set-up adapted to the pulsed excitation and to the detection of the resulting transient probe modifications. Experiments using this new method are presently under way in our laboratory.

Acknowledgments.

We are grateful to E. Hughes for careful reading of the manuscript. One of us (M. L.) acknowledges financial support from the Direction des Recherches Etudes et Techniques (Grant n° 86/1415).

Appendix A.

Throughout this paper, we assume that the system undergoes only step-by-step processes. Taking advantage of the strong collisional broadening of the 6S-6P$_{3/2}$ coherence, we omit the coherent two-photon (Raman) effect [27, 9]. Appendix A, aiming at establishing this assumption on a firm basis, is devoted to a calculation of the inhibited fluorescence signal including the coherent two-photon effect. For the sake of simplicity, we omit the angular degeneracy of the levels, as well as the hyperfine structure.

1. The steady-state equations for the system.

As sketched on figure (13), we now call $\omega_i/2\pi$, $\omega_r/2\pi$, and $\omega_{7P}/2\pi$ the frequencies of the 6S-7S forbidden transition, of the 6S-$6P_{3/2}$ resonance transition, and of the 7S-$6P_{3/2}$ transition used for detection respectively. We call γ_i, γ_r, and γ the damping rates of the corresponding coherences. The frequency of the excitation (detection) laser is denoted $\omega_{e(d)}/2\pi$, and we define $\Delta\omega \equiv \omega_e - \omega_d$.

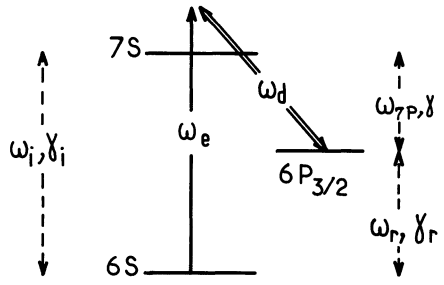

Fig. 13. — Simplified level diagram with the notations used in appendix A.

We consider the steady state of the system. The populations n_6, n_7, and n_P of the 6S, 7S, and $6P_{3/2}$ states are constant in time. The coherences ρ_{76}, ρ_{7P}, ρ_{P6} (in the interaction representation) oscillate, under the action of the laser beams, as

$$\rho_{76}(t, \nu) = \tilde{\rho}_{76}\, e^{-i(\omega_e - \omega_i - 2.72\,\nu)t},$$
$$\rho_{7P}(t, \nu) = \tilde{\rho}_{7P}\, e^{-i(\omega_d - \omega_{7P} - \nu)t},$$
$$\rho_{P6}(t, \nu) = \tilde{\rho}_{P6}\, e^{-i(\Delta\omega - \omega_r - 1.72\,\nu)t},$$

where the $\tilde{\rho}_{ij}$'s are constant in time. Since the two laser beams propagate in the same direction, the Doppler shifts have identical signs. The steady state equations are written as

$$\{i(\omega_e - \omega_i - 2.72\,\nu) - \gamma_i\}\,\tilde{\rho}_{76} + \frac{id\mathcal{E}_e}{2\hbar}(n_6 - n_7) + \frac{iD\mathcal{E}_d}{2\hbar}\tilde{\rho}_{P6} = 0 \qquad (A.1)$$

$$\{i(\omega_d - \omega_{7P} - \nu) - \gamma\}\,\tilde{\rho}_{7P} + \frac{iD\mathcal{E}_d}{2\hbar}(n_P - n_7) + \frac{id\mathcal{E}_e}{2\hbar}\tilde{\rho}^*_{P6} = 0 \qquad (A.2)$$

$$\{i(\Delta\omega - \omega_r - 1.72\,\nu) - \gamma_r\}\,\tilde{\rho}_{P6} + \frac{iD\mathcal{E}_d}{2\hbar}\tilde{\rho}_{76} + \frac{id\mathcal{E}_e}{2\hbar}\tilde{\rho}^*_{7P} = 0 \qquad (A.3)$$

$$-\Gamma_{7S}\,n_7 + \left(\frac{id\mathcal{E}_e}{2\hbar}\tilde{\rho}^*_{76} + \text{c.c.}\right) + \left(\frac{iD\mathcal{E}_d}{2\hbar}\tilde{\rho}^*_{7P} + \text{c.c.}\right) = 0 \qquad (A.4)$$

$$\frac{2}{3}\Gamma_{7S}\,n_7 - (\Gamma_P + \Gamma^{coll})\,n_p + \Gamma^{coll} f(\nu)\,\bar{n}_p - \left(\frac{iD\mathcal{E}_d}{2\hbar}\tilde{\rho}^*_{7P} + \text{c.c.}\right) = 0\,. \qquad (A.5)$$

Here d and D are the dipole matrix elements of the forbidden transition and of the 7S-$6P_{3/2}$ transition respectively ($d \ll D$). The damping rates of the 7S population, of the $6P_{3/2}$ population, and the collisional redistribution rate in the $6P_{3/2}$ state are defined as in section 2, and are noted Γ_{7S}, Γ_P, and Γ^{coll} respectively. At the lowest nonzero order of the

forbidden transition (§ 1.3.iii), n_6 remains unaffected (i.e. $n_6 = n_{Cs}\, f(\nu)$) ; in equation (A.1), n_7 is negligible as compared to n_6 ; in equation (A.3), the last term is negligible as compared to the other.

A relation between $\tilde{\rho}_{P6}$ and $\tilde{\rho}_{76}$ is thus obtained. Carrying this relation in (A.1), one finds that the frequency and width of the forbidden transition are modified by the two-photon effect according to

$$\omega_i' \equiv \omega_i + \left(\frac{D\mathcal{E}_d}{2\hbar}\right)^2 \frac{\Delta\omega - \omega_r - 1.72\,\nu}{\gamma_r^2 + (\Delta\omega - \omega_r - 1.72\,\nu)^2} \tag{A.6}$$

$$\gamma_i' \equiv \gamma_i + \left(\frac{D\mathcal{E}_d}{2\hbar}\right)^2 \frac{\gamma_r}{\gamma_r^2 + (\Delta\omega - \omega_r - 1.72\,\nu)^2}\,. \tag{A.7}$$

Equations (A.1) to (A.3) allow one to eliminate the coherences and, from equations (A.4) and (A.5), one obtains the master equations for the populations

$$(\Gamma_{7S} + R(\nu))\, n_7 - R(\nu)\, n_P = \Lambda g'(\nu) - \Lambda^{coh}(\nu) \tag{A.8}$$

$$-\left(\frac{2}{3}\Gamma_{7S} + R(\nu)\right) n_7 + (\Gamma_P + \Gamma^{coll} + R(\nu))\, n_P - \Gamma^{coll} f(\nu)\, \bar{n}_P = \Lambda^{coh}(\nu) \tag{A.9}$$

where

$$R(\nu) = 2\left(\frac{D\mathcal{E}_d}{2\hbar}\right)^2 \frac{\gamma}{(\omega_d - \omega_{7P} - \nu)^2 + \gamma^2}$$

$$\Lambda g'(\nu) = 2\, n_6 \left(\frac{d\mathcal{E}_e}{2\hbar}\right)^2 \frac{\gamma_i'}{(\omega_e - \omega_i' - 2.72\,\nu)^2 + \gamma_i'^2}$$

$$\Lambda^{coh}(\nu) = -2\, n_6 \left(\frac{d\mathcal{E}_e}{2\hbar}\right)^2 \left(\frac{D\mathcal{E}_d}{2\hbar}\right)^2 \times$$

$$\times\, \mathrm{Im}\left\{\frac{1}{\omega_d - \omega_{7P} - \nu - i\gamma} \times \frac{1}{\Delta\omega - \omega_r - 1.72\,\nu + i\gamma_r} \times \frac{1}{\omega_e - \omega_i' - 2.72\,\nu + i\gamma_i'}\right\}.$$

The excitation rate $\Lambda g'(\nu)$ now replaces $\Lambda_F(\nu)$ (Eqs. (8)). The distribution $g'(\nu)$ coincides with $g(\nu)$ in absence of the probe beam, but is modified by the coherent effect through ω_i' and γ_i' (Eqs. (A.6) and (A.7)). $\Lambda^{coh}(\nu)$ plays the rôle of a source term for the population difference $n_P - n_7$. Even when neither $g'(\nu)$ nor $R(\nu)$ is resonant (that is, when neither laser is resonant for a single-photon transition), $\Lambda^{coh}(\nu)$ acquires a resonant behaviour for a velocity group such that $\Delta\omega \equiv \omega_e - \omega_d = \omega_r + 1.72\,\nu$ (two-photon resonance).

Before solving equations (A.8) and (A.9), let us prove that, despite the modifications of the frequency and width of the forbidden transition (Eqs. (A.6) and (A.7)), the normalization relation $\int g'(\nu)\,d\nu = 1$ is not affected by the presence of the probe beam. Assuming, as in section 2, that γ_i' is small as compared to the Doppler width, $\int g'(\nu)\,d\nu$ can be written as a quantity of the form

$$\mathrm{Re}\left\{\int_{-\infty}^{+\infty} \left(1 + ix + \frac{a}{1 + ib(x-c)}\right)^{-1} dx\right\},$$

where a, which is proportional to the saturation parameter s, b, and c are real ($a, b > 0$). One can easily show that this quantity does not depend on s : its derivative with respect to a is the integral of a quantity whose poles lie in the lower half of the complex plane (as soon as $a > -1$). Therefore the derivative with respect to s is zero and the result $\int g'(\nu)\,d\nu = 1$, obvious for $s = 0$, remains true at any saturation level.

2. Lowest order solution.

The calculation is very similar to that of § 3.1. The presence of Λ^{coh} in (A.8) and (A.9) simply results in an additional term $-\int \Lambda^{coh}(\nu)\,d\nu/\Lambda$ in the previously obtained solution (Eq. (27)). We define

$$\delta \equiv (\omega_d - \omega_{7P}) + (\omega_e - \omega_i)/2.72 = \nu_e - \nu_d$$
$$\gamma_1 \equiv (1.72\,\gamma + \gamma_r)/2.72$$
$$\gamma_2 \equiv \gamma + \gamma_i/2.72\,.$$

A residue integration (omitting higher orders) gives

$$\int \Lambda^{coh}(\nu)\,d\nu\,/\Lambda = \frac{s(\gamma_1\,\gamma_2 - \delta^2)\,\gamma\Gamma_{7S}}{2.72(\gamma_1^2 + \delta^2)\,(\gamma_2^2 + \delta^2)}\,.$$

At the center of a resonance, the ratio of the coherent to the step-by-step contributions is easily calculated to be

$$\sigma^{coh} = \frac{\Gamma_{7S}\,\gamma}{2.72\,\gamma_1\,\gamma_2}\Big/\left(1 - \frac{2\,C_{F'}^{F}\,\Gamma_{7S}/3}{\Gamma_P + \Gamma^{coll}}\right) = \begin{cases} 8\,\% \text{ for } n_{Cs} = 2 \times 10^{14}\ \text{cm}^{-3} \\ 30\,\% \text{ for } n_{Cs} < 10^{13}\ \text{cm}^{-3}\,. \end{cases}$$

To take into account the hyperfine structure of the 7S-6P$_{3/2}$ transition, we inserted in the denominator the usual oscillator strength $C_{F'}^{F}$. Since γ is not very different from γ_r, σ^{coh} turns out to be roughly equal to $(\omega_{7P}/\omega_i)\,(\Gamma_{7S}/\gamma_r)$, as previously indicated. Owing to the reduction factor $\omega_i/\omega_{7P} \simeq 2.72$, the stepwise process always dominates, even when the 6S-6P$_{3/2}$ coherence is not strongly damped by collisions.

Figure 14a and b shows the calculated spectral shape of the inhibited fluorescence holes, with and without the contribution of the coherent effect, in the conditions where the coherent effect is maximum (30 %). The coherent effect results in a smaller width and a larger depth for the holes.

The computer code previously used to extract γ from experimental spectra, was run later with the theoretical shape including the coherent effect. For all values of the Cs density for which spectra were recorded, the coherent effect modified the best fit value of γ by only $\simeq 1.5$ MHz. Hence the reported value for the collisional broadening (Eq. (41)) is in practice not affected by the coherent effect. The values of Γ_P are not affected either, since the coherent effect is not involved in the 6P$_{3/2} \rightarrow$ 7S reexcitation rate.

Let us briefly mention that, if the two beams were propagating in opposite directions, then the three poles of $\Lambda^{coh}(\nu)$ would lie in the lower half of the complex plane. The integral $\int \Lambda^{coh}(\nu)\,d\nu$ would vanish, and coherent effect would give no contribution at the lowest order. The disappearance of the coherent effect for counterpropagating beams has been verified by other authors in conditions where the effect for copropagating beams is large [28].

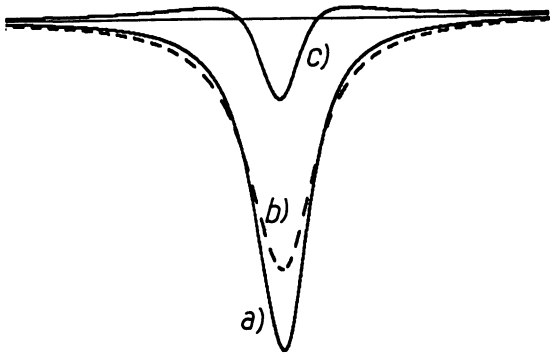

Fig. 14. — Spectral shape of the inhibited fluorescence hole with (a) and without (b) the two-photon contribution. Curve c) is the spectral shape of the two-photon contribution.

3. Non-perturbative solution.

The non-perturbative resolution of equations (A.8), (A.9) follows the same method as in § 3.2, and results in the substitution $\mathcal{G} \to \mathcal{G} + \mathcal{G}^{coh}$ in equation (33), with

$$\mathcal{G}^{coh}(\omega_d) = \int \frac{\Lambda^{coh}(\nu)/\Lambda}{1 + R(\nu)\,(3+\kappa)/3\,\Gamma_{7S}}\,d\nu\,.$$

We find that $\mathcal{G}^{coh}/\mathcal{G}$ does not vary significantly between weak and strong saturation.

A large Autler-Townes effect [29] could in principle result in an observable splitting of the sharp function shapes $\mathcal{G}(\omega_d)$ and $\mathcal{G}^{coh}(\omega_d)$. In fact, we have found that the Autler-Townes splitting of $g(\nu)$ is always small enough to vanish when velocity integrations are performed. For reasonable values of the collisional damping rates, a non-zero splitting is predicted for $\mathcal{G}^{coh}(\omega_d)$; but the amplitude of the splitting remains negligible as compared to the spectral width of the two-photon contribution.

So our conclusion is that two-photon effects cannot lead to an observable splitting of the inhibited fluorescence holes, and this matches the results of the experiments performed on the forbidden three-level system in quite a wide range of Cs densities (where γ and γ_r ranged from their radiative limits to $\simeq 8$ times these limits).

Appendix B.

On several occasions during the calculations, we have used the operator $\vec{\mathcal{C}}\begin{matrix}F\\ \downarrow\\ F'\end{matrix}$ (defined by (Eq. (16)) which acts inside the $7S_{1/2}F$ level. We also defined $\vec{\mathcal{C}}\begin{matrix}F\\ \downarrow\\ F'\end{matrix}$ (Eq. (17)) which acts inside $6P_{3/2}F'$. Then the quantities to be calculated (e.g. the radiative transition rates) are of the form $\mathrm{tr}\,\{\rho\hat{u}\,.\,\vec{\mathcal{C}}\,.\hat{v}\}$, where $\hat{u}$, $\hat{v}$, are polarization vectors, and ρ is the density matrix in the 7SF or $6P_{3/2}F'$ levels. The calculations are greatly simplified when the operators $\vec{\mathcal{C}}$, of rank 2, are developed on the basis formed by the irreducible tensor operators $\vec{F}^{(0)}$, $\vec{F}^{(1)}$, and $\vec{F}^{(2)}$ defined by equations (18). In this appendix we first calculate the coefficients of the

decomposition in the general case of a transition between any two levels of an arbitrary atom and then apply the results to the $7S \leftrightarrow 6P_{3/2}$ transitions of Cs.

1. General case.

We consider an arbitrary $\tau j F \to \tau' j' F'$ transition of an atom of nuclear spin I. We define

$$\vec{\mathcal{C}} \begin{matrix} F \\ \downarrow \\ F' \end{matrix} \equiv \mathbb{P}(\tau j F)\, \mathfrak{D}\, \mathbb{P}(\tau' j' F')\, \mathfrak{D}\, \mathbb{P}(\tau j F) \tag{B.1}$$

($\tau j F$ is assumed to be the upper level of the transition), and

$$\vec{\mathcal{C}} \begin{matrix} F \\ \uparrow \\ F' \end{matrix} \equiv \mathbb{P}(\tau' j' F')\, \mathfrak{D}\, \mathbb{P}(\tau j F)\, \mathfrak{D}\, \mathbb{P}(\tau' j' F') \tag{B.2}$$

($\mathfrak{D} = -|e|\,\mathbf{r}$ is the electric dipole operator ; $\mathbb{P}(\tau j F)$ is the projector on the multiplicity F of level τj). We now calculate

$$\mathcal{C}_{qq'} = \sum_{m_1 m_2 \mu} |\tau j, Fm_1\rangle \langle \tau j, Fm_1 | \mathfrak{D}_q | \tau' j', F' \mu \rangle \times \langle \tau' j', F' \mu | \mathfrak{D}_{q'} | \tau j, Fm_2 \rangle \langle \tau j, Fm_2 |.$$

We use the Wigner-Eckart theorem ([30], App. C), written in the form

$$\langle (j_1, j_2) jm | T_q^{(K)} | (j_1', j_2) j' m' \rangle = \langle j_1 \| T^{(K)} \| j_1' \rangle \times$$
$$\times (-1)^{-j_2 - j_1 + m} \begin{Bmatrix} j' & K & j \\ j_1 & j_2 & j_1' \end{Bmatrix} \sqrt{(2j+1)(2j'+1)} \begin{pmatrix} j' & K & j \\ m' & q & -m \end{pmatrix}.$$

(the operator $T^{(K)}$ is assumed to act only in the subspace of angular momentum $\mathbf{j}_1$). It is convenient to write

$$\mathcal{C}_{qq'} = \mathcal{A} \begin{matrix} F \\ \downarrow \\ F' \end{matrix} \frac{|\langle \tau j \| \mathfrak{D} \| \tau' j' \rangle|^2}{F(F+1)(2F+1)} \mathcal{T}_{qq'} \tag{B.3}$$

where

$$\mathcal{A} \begin{matrix} F \\ \downarrow \\ F' \end{matrix} \equiv (2F+1)(2F'+1) \begin{Bmatrix} F & 1 & F' \\ j' & I & j \end{Bmatrix}^2. \tag{B.4}$$

The spherical coordinates $\mathcal{T}_{qq'}$ are then equal to

$$\mathcal{T}_{qq'} = (-1)^q F(F+1)(2F+1) \sum_m |F, m\rangle \langle F, m-q-q'| \times$$
$$\times \begin{pmatrix} F' & 1 & F \\ m-q & q & -m \end{pmatrix} \begin{pmatrix} F & 1 & F' \\ m-q-q' & q' & -m-q \end{pmatrix}. \tag{B.5}$$

From $\vec{\mathcal{T}}$ one can construct three irreducible tensor operators, of rank 0, 1, and 2 following the three terms of the identity

$$\mathcal{T}_{ij} = (1/3)\,\delta_{ij} \sum_k \mathcal{T}_{kk} + (1/2)[\mathcal{T}_{ij} - \mathcal{T}_{ji}] + \left\{(1/2)[\mathcal{T}_{ij} + \mathcal{T}_{ji}] - (1/3)\,\delta_{ij} \sum_k \mathcal{T}_{kk}\right\}$$

(the coefficients $\mathfrak{F}_{ij}$ are the cartesian coordinates of $\vec{\mathfrak{F}}$). The result is written

$$\vec{\mathfrak{F}} = \vec{\mathbb{F}}^{(0)} + ia \underset{F'}{\overset{F}{\downarrow}} \vec{\mathbb{F}}^{(1)} + b \underset{F'}{\overset{F}{\downarrow}} \vec{\mathbb{F}}^{(2)} . \tag{B.6}$$

Where $a\downarrow$ and $b\downarrow$ are real coefficients depending only on F and F' :

$$a \underset{F-1}{\overset{F}{\downarrow}} = -F ; \qquad b \underset{F-1}{\overset{F}{\downarrow}} = -\frac{F}{2F+3} ; \tag{B.7a}$$

$$a \underset{F}{\overset{F}{\downarrow}} = 1 ; \qquad b \underset{F}{\overset{F}{\downarrow}} = 1 ; \tag{B.7b}$$

$$a \underset{F+1}{\overset{F}{\downarrow}} = F+1 ; \quad b \underset{F+1}{\overset{F}{\downarrow}} = -\frac{F+1}{2F-1} . \tag{B.7c}$$

Finally, from equations (B.3) and (B.6), one obtains the expression for $\vec{\mathcal{C}} \underset{F'}{\overset{F}{\downarrow}}$:

$$\vec{\mathcal{C}} \underset{F'}{\overset{F}{\downarrow}} = \mathcal{A} \underset{F'}{\overset{F}{\downarrow}} \frac{|\langle \tau j \| \mathfrak{D} \| \tau' j' \rangle|^2}{F(F+1)(2F+1)} \mathbb{P}(\tau j F) \left\{ \vec{\mathbb{F}}^{(0)} + ia \underset{F'}{\overset{F}{\downarrow}} \vec{\mathbb{F}}^{(1)} + b \underset{F'}{\overset{F}{\downarrow}} \vec{\mathbb{F}}^{(2)} \right\} .$$

$\mathcal{A} \underset{F'}{\overset{F}{\downarrow}}$ involve $6j$ coefficients (Eq. B.4)). Let us give the expressions of the 6 j's for a $j = 1/2$ level (often considered in alkali atoms).

$$\begin{Bmatrix} F & 1 & F' \\ j' & I & 1/2 \end{Bmatrix}^2 =$$

$$= \begin{cases} (F'-I+3/2)(F'+I-1/2)/[12I(2I+1)] & \text{if } j'=1/2 \text{ and } F=I-1/2 \\ (F'+I+5/2)(-F'+I+3/2)/[12(I+1)(2I+1)] & \text{if } j'=1/2 \text{ and } F=I+1/2 \\ (F'+I+5/2)(-F'+I+3/2)/[24I(2I+1)] & \text{if } j'=3/2 \text{ and } F=I-1/2 \\ (F'-I+3/2)(F'+I-1/2)/[24(I+1)(2I+1)] & \text{if } j'=3/2 \text{ and } F=I+1/2. \end{cases}$$

We now consider the reverse (absorption) process $\tau' j' F' \rightarrow \tau j F$. The $\vec{\mathcal{C}} \underset{F'}{\overset{F}{\uparrow}}$ operator (Eq. (B.2)) is developed according to

$$\vec{\mathcal{C}} \underset{F'}{\overset{F}{\uparrow}} = \mathcal{A} \underset{F'}{\overset{F}{\uparrow}} \frac{|\langle \tau j \| \mathfrak{D} \| \tau' j' \rangle|^2}{F'(F'+1)(2F'+1)} \times \mathbb{P}(\tau' j' F') \left\{ \vec{\mathbb{F}}^{(0)} + ia \underset{F'}{\overset{F}{\uparrow}} \vec{\mathbb{F}}^{(1)} + b \underset{F'}{\overset{F}{\uparrow}} \vec{\mathbb{F}}^{(2)} \right\} .$$

The $\mathcal{A}\uparrow$, $a\uparrow$, and $b\uparrow$ coefficients are related to the $\mathcal{A}\downarrow$, $a\downarrow$, and $b\downarrow$ appearing in equation (B.7). Using trace invariance properties, one easily shows that

$$\mathcal{A} \underset{F'}{\overset{F}{\uparrow}} = \mathcal{A} \underset{F'}{\overset{F}{\downarrow}} . \tag{B.8}$$

We further take into account the relation

$$[(\mathfrak{D}\cdot\mathbf{u}),\,(\mathbf{F}\cdot\mathbf{v})] = i\,(\mathbf{u}\wedge\mathbf{v})\cdot\mathfrak{D}\,,$$

which holds since $\mathfrak{D}$ is an irreducible tensor operator of rank 1, and obtain [19]

$$a\,{}^{F}_{F'}\uparrow \;=\; 2 - a\,{}^{F}_{F'}\downarrow \tag{B.9}$$

$$b\,{}^{F}_{F'}\uparrow \;=\; b\,{}^{F}_{F'}\downarrow \left\{\frac{4F(F+1)-3}{4F'(F'+1)-3}\right\} + 5\left\{\frac{F(F+1)-F'(F'+1)}{4F'(F'+1)-3}\right\}. \tag{B.10}$$

2. The $7S\text{-}6P_{3/2}$ transitions of the Cs atom.

We now apply equations (B.4), (B.7), (B.9), and (B.10) to the $7S_{1/2}\ F \rightarrow 6P_{3/2}\ F'$ transitions of ^{133}Cs ($I = 7/2$). The corresponding values of the $\mathcal{A}$, a, and b coefficients are listed below (in view of Eq. (B.8), we omit the arrow for coefficients $\mathcal{A}$) :

$\mathcal{A}\,{}^{F}_{F'}$

$F' =$	$F+1$	F	$F-1$
$F = 3$	$\frac{15}{16}$	$\frac{21}{16}$	$\frac{20}{16}$
$F = 4$	$\frac{44}{16}$	$\frac{21}{16}$	$\frac{7}{16}$

$a\,{}^{F}_{F'}\downarrow$

$F' =$	$F+1$	F	$F-1$
$F = 3$	-3	1	4
$F = 4$	-4	1	5

$a\,{}^{F}_{F'}\uparrow$

$F' =$	$F+1$	F	$F-1$
$F = 3$	5	1	2
$F = 4$	6	1	3

$b\,{}^{F}_{F'}\downarrow$

$F' =$	$F+1$	F	$F-1$
$F = 3$	$-\frac{1}{3}$	1	$-\frac{4}{5}$
$F = 4$	$-\frac{4}{11}$	1	$-\frac{5}{7}$

$b \uparrow$ F / F′	$F' = F+1$	F	$F-1$
$F = 3$	$-\frac{5}{7}$	1	$-\frac{2}{7}$
$F = 4$	$-\frac{2}{3}$	1	$-\frac{1}{3}$

Finally we define the coefficients $C^{F}_{F'}$ by

$$C^{F}_{F'} \equiv \frac{2}{2F+1} \mathcal{A}^{F}_{F'}$$

C F / F′	$F' = F+1$	F	$F-1$
$F = 3$	$\frac{15}{56}$	$\frac{21}{56}$	$\frac{20}{56}$
$F = 4$	$\frac{44}{72}$	$\frac{21}{72}$	$\frac{7}{72}$

Defining $C^{3}_{5} = C^{4}_{2} = 0$, we obtain the simple summations rules

$$\sum_{F'} C^{F}_{F'} = 1 , \quad F = 3 \quad \text{or} \quad 4 .$$

Appendix C.

In this appendix we summarize the non-perturbative calculation of the helicity-dependent fluorescence signal. Our treatment includes the alignment induced by the probe laser.

We express the density matrix in terms of the populations in 7SF and 6P$_{3/2}$ F′, and of the orientation and alignment in 7SF (Eqs. (44), (45)). Defining $\mathbb{F} \equiv F(F+1)/3$ and $F_k \equiv \mathbf{F} \cdot \hat{k}$, we write

$$\rho(\nu) = \left\{ n_{7F} + \frac{F_k}{\mathbb{F}} p_{7F} + 5 \left(\frac{1 - F_k^2/\mathbb{F}}{4 - 1/\mathbb{F}} \right) q_{7F} \right\} \times \frac{\mathbb{P}(7SF)}{2F+1} + \sum_{F'} n_{PF'} \frac{\mathbb{P}(6P_{3/2}F')}{2F'+1} .$$

For simplicity, we now drop the explicit ν-dependence of the variables n_{7F}, p_{7F}, q_{7F}, and $n_{PF'}$. Within the assumptions presented and discussed in § 4.2, these quantities obey the steady-state equations :

$$-\Gamma_{7S} n_{7F} - \sum_{F'} R^{F}_{F'}(\nu) \left(\lambda_{00} n_{7F} + \xi_d \lambda_{01} p_{7F} + \lambda_{02} q_{7F} - \mu^{F}_{F'} n_{PF'} \right) = 0 \qquad \text{(C.1a)}$$

$$-\Gamma_{7S} p_{7F} + \xi_e \Lambda^{(1)} g(\nu) - \sum_{F'} R^{F}_{F'}(\nu) \left(\xi_d \lambda_{10} n_{7F} + \lambda_{11} p_{7F} + \xi_d \lambda_{12} q_{7F} - \xi_d \mu^{F}_{F'} \lambda_{10} n_{PF'} \right) = 0 \qquad \text{(C.1b)}$$

$$-\Gamma_{7S} q_{7F} - \sum_{F'} R^{F}_{F'}(\nu) \left(\lambda_{20} n_{7F} + \xi_d \lambda_{21} p_{7F} + \lambda_{22} q_{7F} - \mu^{F}_{F'} \lambda_{20} n_{PF'} \right) = 0 \qquad \text{(C.1c)}$$

$$-(\Gamma_p + \Gamma^{coll})\, n_{PF'} + \Gamma^{coll} w_{F'} f(\nu)\, \bar{n}_p + \frac{2}{3}\Gamma_{7S} C^F_{F'} n_{7F} + \\ + R^F_{F'}(\nu)\,(\lambda_{00} n_{7F} + \xi_d \lambda_{01} p_{7F} + \lambda_{02} q_{7F} - \mu^F_{F'} n_{PF'}) = 0 \quad \text{(C.1d)}$$

where the λ_{ij}'s are functions of F and F' :

$$\lambda_{00} \equiv 1 ; \qquad \lambda_{01} \equiv \underset{F'}{\overset{F}{a\downarrow}} /2\,\mathbb{F} ; \qquad \lambda_{02} \equiv \underset{F'}{\overset{F}{b\downarrow}} /2 ;$$

$$\lambda_{10} \equiv \underset{F'}{\overset{F}{a\downarrow}} /2 ; \quad \lambda_{11} \equiv 1 - \underset{F'}{\overset{F}{b\downarrow}} \left(4 - \frac{1}{\mathbb{F}}\right)/10 ; \quad \lambda_{12} \equiv - \underset{F'}{\overset{F}{a\downarrow}} /2 ;$$

$$\lambda_{20} \equiv \underset{F'}{\overset{F}{b\downarrow}} \left(4 - \frac{1}{\mathbb{F}}\right)/10 ; \; \lambda_{21} \equiv - \underset{F'}{\overset{F}{a\downarrow}} \left(4 - \frac{1}{\mathbb{F}}\right)/10\,\mathbb{F} ; \; \lambda_{22} \equiv 1 - \underset{F'}{\overset{F}{b\downarrow}} \left(\frac{16\,\mathbb{F}^2 - 24\,\mathbb{F} + 5}{14\,\mathbb{F}(4\,\mathbb{F} - 1)}\right).$$

We introduce

$$\mathcal{R}_{0j} = \sum_{F'} \lambda_{0j} R^F_{F'}(\nu)$$

$$\mathcal{R}_{i0} = \sum_{F'} \lambda_{i0} R^F_{F'}(\nu) \left\{1 - \frac{\mu^F_{F'}[2\,\Gamma_{7S} C^F_{F'}/3 + R^F_{F'}(\nu)]}{\Gamma_p + \Gamma^{coll} + \mu^F_{F'} R^F_{F'}(\nu)}\right\} \quad \text{if} \quad i \neq 0$$

$$\mathcal{R}_{ij} = \sum_{F'} R^F_{F'}(\nu) \left\{\lambda_{ij} - \frac{\mu^F_{F'} \lambda_{i0} \lambda_{0j} R^F_{F'}(\nu)}{\Gamma_p + \Gamma^{coll} + \mu^F_{F'} R^F_{F'}(\nu)}\right\} \quad \text{if} \quad i \neq 0 \quad \text{and} \quad j \neq 0$$

$$\bar{\mathcal{R}}_i = \sum_{F'} R^F_{F'}(\nu)\, \lambda_{i0}\, \Gamma^{coll} / [\Gamma^{coll} + \Gamma_p + \mu^F_{F'} R^F_{F'}(\nu)] \quad \text{if} \quad i \neq 0 .$$

Equations (C.1) then become

$$(\Gamma_{7S} + \mathcal{R}_{00})\, n_{7F} + \xi_d \mathcal{R}_{01} p_{7F} + \mathcal{R}_{02} q_{7F} - \sum_{F'} R^F_{F'}(\nu)\, \mu^F_{F'} n_{PF'} = 0 \quad \text{(C.2a)}$$

$$\xi_d \mathcal{R}_{10} n_{7F} + (\Gamma_{7S} + \mathcal{R}_{11})\, p_{7F} + \xi_d \mathcal{R}_{12} q_{7F} - \xi_d w_F \bar{\mathcal{R}}_1 \bar{n}_p f(\nu) = \xi_e \Lambda^{(1)} g(\nu) \quad \text{(C.2b)}$$

$$\mathcal{R}_{20} n_{7F} + \xi_d \mathcal{R}_{21} p_{7F} + (\Gamma_{7S} + \mathcal{R}_{22})\, q_{7F} - w_F \bar{\mathcal{R}}_2 \bar{n}_p f(\nu) = 0 \quad \text{(C.2c)}$$

$$\left[\frac{2}{3}\Gamma_{7S} C^F_{F'} + R^F_{F'}(\nu)\right] n_{7F} + \xi_d \lambda_{01} \mathcal{R}^F_{F'}(\nu)\, p_{7F} + \lambda_{02} R^F_{F'}(\nu)\, q_{7F} - \\ - [\Gamma^{coll} + \Gamma_p + \mu^F_{F'} R^F_{F'}(\nu)]\, n_{PF'} + \Gamma^{coll} w_{F'} f(\nu)\, \bar{n}_p = 0 . \quad \text{(C.2d)}$$

Summing equation (C.2d) over F' and subtracting from equation (C.2a), one obtains, after velocity integration, the simple conservation relation mentioned in the text (Eq. (46)). Then straightforward substitution of p_{7F}, q_{7F}, and n_{7F} leads to

$$\left\{I + J - \left(1 - \frac{w_F \Gamma_{7S}}{3\,\Gamma^{coll}}\right) I'\right\} \frac{\Gamma^{coll}}{\Gamma_p + \Gamma^{coll}} f(\nu)\, \bar{n}_p + \frac{I_\xi \xi_d \xi_e \Lambda^{(1)} g(\nu)}{\Gamma_p + \Gamma^{coll}} = (1 + I - I') \sum_{F'} n_{PF'}$$

in which

$$I \equiv (\Gamma^{\text{coll}} + \Gamma_p) \sum_{F'} \frac{2\,C^F_{F'} + 3\,R^F_{F'}(\nu)/\Gamma_{7S}}{\Gamma^{\text{coll}} + \Gamma_p + \mu^F_{F'} R^F_{F'}(\nu)} \left\{ 1 - \frac{\lambda_{02} R^F_{F'}(\nu)\,\mathcal{R}_{20}}{(\Gamma_{7S} + \mathcal{R}_{22}) \left(\frac{2}{3}\Gamma_{7S} C^F_{F'} + R^F_{F'}(\nu) \right)} \right\},$$

$$J \equiv (\Gamma^{\text{coll}} + \Gamma_p) \sum_{F'} \frac{w_{F'}}{\Gamma^{\text{coll}} + \Gamma_p + \mu^F_{F'} R^F_{F'}(\nu)} \left\{ 1 + \frac{\lambda_{02} R^F_{F'}(\nu)\,\mu^F_{F'}\,\mathcal{R}_{20}}{\Gamma^{\text{coll}}(\Gamma_{7S} + \mathcal{R}_{22})} \right\},$$

$$I_\xi \equiv \frac{(\Gamma^{\text{coll}} + \Gamma_p)/(\Gamma_{7S} + \mathcal{R}_{11})}{\left\{ 1 - \frac{\xi_d^2 \mathcal{R}_{12}\,\mathcal{R}_{21}}{(\Gamma_{7S} + \mathcal{R}_{22})(\Gamma_{7S} + \mathcal{R}_{11})} \right\}} \sum_{F'} \frac{\lambda_{01} R^F_{F'}(\nu)}{\Gamma^{\text{coll}} + \Gamma_p + \mu^F_{F'} R^F_{F'}(\nu)} \left\{ 1 - \frac{\lambda_{02}\,\mathcal{R}_{21}}{\lambda_{01}(\Gamma_{7S} + \mathcal{R}_{22})} \right\},$$

$$I'_\xi \equiv \frac{3\,\xi_d^2 \mathcal{R}_{10}}{\Gamma_{7S}} \left\{ 1 - \frac{\mathcal{R}_{12}\,\mathcal{R}_{20}}{(\Gamma_{7S} + \mathcal{R}_{22})\,\mathcal{R}_{10}} \right\} I_\xi .$$

These expressions for $I(\nu)$ and $J(\nu)$ differ from equations (30) by factors (curly braces) which originate in the alignment and bring higher-order corrections. Then, one easily obtains $\bar{n}_p$, and (using Eq. (46)) $\bar{n}_7$:

$$\bar{n}_7 = \xi_d\,\xi_e \left(\frac{\Lambda^{(1)}}{\Gamma_{7S}} \right) \frac{-\mathcal{G}_\xi}{1 + \mathcal{F}_\xi/2} \tag{C.3}$$

where

$$\mathcal{G}_\xi \equiv 3 \int_{-\infty}^{+\infty} \frac{I_\xi}{1 + I - I'_\xi}\, g(\nu)\,\mathrm{d}\nu , \tag{C.4a}$$

$$\mathcal{F}_\xi \equiv 2\,\frac{\Gamma^{\text{coll}}}{\Gamma_p} \int_{-\infty}^{+\infty} \frac{1 - J - w_F\,\Gamma_{7S}\,I'_\xi/3\,\Gamma^{\text{coll}}}{1 + I - I'_\xi}\, f(\nu)\,\mathrm{d}\nu . \tag{C.4b}$$

In order to obtain an (approximate) analytical expression for $\mathcal{G}_\xi$ and $\mathcal{F}_\xi$, we use the same approximation as in section 3. Then $\mathcal{G}_\xi$ is simply given by $3\,I_\xi/(1 + I - I'_\xi)\big|_{\nu = \nu_e}$. The quantities I, I'_ξ and I_ξ can be expressed in terms of the functions $\mathcal{L}_{F'}(\Delta^e_{F'})$ (Eq. (36)), of the bare lorentzian shape $L_{F'}(\Delta^e_{F'}) \equiv C^F_{F'}/(1 + \Delta^{e2}_{F'})$, and of the frequency-dependent coefficients $\lambda^0_{ij} \equiv \lambda_{ij} - \lambda_{i0}\,\lambda_{0j}/(1 + \kappa s \mu^F_{F'} L_{F'})$. This notation allows us to emphasize the modifications introduced by taking the alignment into account. We obtain

$$I = \sum_{F'} \frac{2\,C^F_{F'} + 3\,s\lambda_{00} L_{F'}}{1 + \kappa s \mu^F_{F'} L_{F'}} - \frac{\sum_{F'} s\lambda_{20}\,\mathcal{L}_{F'}}{1 + \sum_{F'} s\lambda^0_{22} L_{F'}} \sum_{F'} \frac{3\,s\,\lambda_{02} L_{F'}}{1 + \kappa s \mu^F_{F'} L_{F'}}$$

$$I_\xi = \frac{\sum_{F'} \frac{sL_{F'}}{1 + \kappa s \mu^F_{F'} L_{F'}}\, sL_{F'} \left\{ \lambda_{01} - \lambda_{02} \frac{\sum_{F'} s\lambda^0_{21} L_{F''}}{1 + \sum_{F''} s\lambda^0_{22} L_{F''}} \right\}}{1 + \sum_{F'} s\lambda^0_{11} L_{F'} - \xi_d^2 \frac{\sum_{F'} s\lambda^0_{12} L_{F'} \times \sum_{F''} s\lambda^0_{21} L_{F'}}{1 + \sum_{F'} s\lambda^0_{22} L_{F'}}}$$

$$I'_\xi = 3\, I_\xi \times \xi_d^2 \left\{ \sum_{F'} s\lambda_{10}\, \mathcal{L}_{F'} - \frac{\sum_{F'} s\lambda_{12}^0\, L_{F'} \times \sum_{F'} s\lambda_{20}\, \mathcal{L}_{F'}}{1 + \sum_{F'} s\lambda_{22}^0\, L_{F'}} \right\} .$$

In these quantities, including the alignment does not contribute by more than 13 % at $s = 1$.

Now, considering equation (C.4b), one notices that $\mathcal{F}_\xi$ is not very different from $\mathcal{F}$ (Eq. (31b)) : $I'_\xi(\nu)$, and the alignment-induced corrections to $I(\nu)$ and $J(\nu)$, only bring small modifications (1 to 15 % at $s = 1$, depending on the transition). Therefore we calculate $\mathcal{F}_\xi - \mathcal{F}$ at the lowest order in these corrections. We also omit the very small fraction of non-thermalized $6P_{3/2}$ atoms (approximations $\kappa s C_{F'}^F \ll 1$ and $\Gamma^{coll} \gg \Gamma_P$). It should be recalled that these approximations will not affect the shape of the resonances, but only their heights. The calculation follows the same assumptions as in the calculation of $\mathcal{F}$, i.e. :

— $f(\nu)$ is assumed to be constant over the width of a resonance ;

— the resonances are supposed to be well resolved.

The resulting expression for $\mathcal{F}_\xi$ is very close to equation (39), except that the weights $1/\pi_{F'}$ have to be replaced by $(1 + \xi_d^2\, \varphi_{1F'} + \varphi_{2F'})/\pi_{F'}$, where

$$\varphi_{iF'} = \frac{3}{8} \frac{(sC_{F'}^F)^2\, \lambda_{i0}\, \lambda_{0i}}{(1 + sC_{F'}^F\, \lambda_{ii})^2} - \frac{\lambda_{i0}\, \lambda_{0i}\, sC_{F'}^F}{1 + sC_{F'}^F\, \lambda_{ii} + \pi_{F'} \sqrt{1 + sC_{F'}^F\, \lambda_{ii}}} , \qquad i = 1, 2 .$$

Finally, the alignment-induced corrections at $s = 1$ amount to less than 13 % in $\mathcal{G}_\xi$ and less than 15 % in $\mathcal{F}_\xi$.

References

[1] BOUCHIAT, M. A. and POTTIER, L., in « Atomic Physics 9 » p. 246 ; eds. R. S. Van Dyck and E. N. Fortson, World Scientific (Singapore 1984).

[2] BOUCHIAT, M. A. and BOUCHIAT, C., *J. Phys. France* **35** (1974) 899 et **36** (1975) 493.

[3] BOUCHIAT, C. and PIKETTY, C. A., *Phys. Lett.* **128B** (1983) 73.

[4] BOUCHIAT, M. A., GUENA, J., HUNTER, L. and POTTIER, L., *Phys. Lett.* **117B** (1982) 358 and **134B** (1984) 463 and *J. Phys. France* **47** (1986) 1709.

[5] GILBERT, S. L. and WIEMAN, C. E., *Phys. Rev.* **A 34** (1986) 792.

[6] BOUCHIAT, M. A., JACQUIER, P., LINTZ, M. and POTTIER, L., *Opt. Commun.* **56** (1985) 100.

[7] BOUCHIAT, C., PIKETTY, C. A. and PIGNON, D., *Nucl. Phys.* **B 221** (1983) 68.

[8] FEUILLADE, C. and BERMAN, P. R., *Phys. Rev.* **A 29** (1984) 1236.

[9] See for instance S. STENHOLM, Foundations of laser spectroscopy (Wiley, New York 1984).

[10] GREGORY, C., *Phys. Rev.* **61** (1942) 465.

[11] CHEN, C. L. and PHELPS, A. V., *Phys. Rev.* **173** (1968) 62.

[12] BOUCHIAT, M. A., GUENA, J., POTTIER, L., *J. Phys. Lett. France* **45** (1984) L523.

[13] HOLSTEIN, T., *Phys. Rev.* **72** (1947) 1212 and **83** (1951) 1159.

[14] LINTZ, M., GUENA, J., JACQUIER, P., POTTIER, L. and BOUCHIAT, M. A., *Europhys. Lett.* **4** (1987) 53.

[15] GUENA, J., LINTZ, M., JACQUIER, P., POTTIER, L. and BOUCHIAT, M. A., *Opt. Commun.* **62** (1987) 97.

[16] KRAUSE, L., *Appl. Opt.* **5** (1966) 1375.

[17] ZEMANSKY, M. W., *Phys. Rev.* **29** (1927) 513.

[18] ZAJONC, A. G. and PHELPS, A. V., *Phys. Rev.* **A 23** (1981) 2479 and references therein.
[19] LINTZ, M., Thèse de Doctorat de l'Université Paris XI (1987).
[20] LAM, L. K., FUJIMOTO, T. and GALLAGHER, A. C., *J. Chem. Phys.* **68** (1978) 3553.
[21] VIGUE, J., Private communication.
[22] DUCLOY, M., GORZA, M. P. and DECOMPS, B., *Opt. Commun.* **8** (1973) 21.
[23] CHEBOTAYEV, V. P., in High Resolution Spectroscopy, Topics in Applied Physics, Vol. 13, ed. K. Shimoda (Springer Verlag, Berlin, 1976) ;
WIEMAN, C. and HÄNSCH, T. W., *Phys. Rev. Lett.* **36** (1976) 1170.
DELSART, C. and KELLER, J. C., *J. Appl. Phys.* **49** (1978) 3662.
PINARD, M., AMINOFF, C. G. and LALOE, F., *Phys. Rev.* **A 19** (1979) 2366.
[24] BOUCHIAT, M. A., GUENA, J., POTTIER, L., *J. Phys. France* **46** (1985) 1897.
[25] HOFFNAGLE, J., ROESCH, L. Ph., TELEGDI, V. L., WEIS, A. and ZEHNDER, A., *Phys. Lett.* **85A** (1981) 143.
BOUCHIAT, M. A., GUENA, J., HUNTER, L. and POTTIER, L., *Opt. Commun.* **45** (1983) 35.
GILBERT, S. L., WATTS, R. N. and WIEMAN, C. E., *Phys. Rev.* **A 27** (1983) 581.
[26] BOUCHIAT, M. A., GUENA, J., JACQUIER, P., LINTZ, M. and POTTIER, L., in « Interaction of radiation with matter — a volume in honour of Pr. A. Gozzini ». (Scuola Normale Superiore, Pisa, Italy.) p. 111.
[27] HÄNSCH, T. and TOSCHEK, P. E., *Z. Phys.* **236** (1970) 213.
[28] LEITE, J. R. R., DUCLOY, M., SANCHEZ, A., SELIGSON, D. and FELD, M. S., *Phys. Rev. Lett.* **39** (1977) 1465.
[29] AUTLER, S. H. et TOWNES, C. H., *Phys. Rev.* **78** (1950) 340 et **100** (1955) 703 ;
COHEN TANNOUDJI, C. and HAROCHE, S., in « Polarisation, Matière et Rayonnement » Ed. Société Française de Physique (Presses Universitaires de France, Paris, 1969) p. 191.
[30] MESSIAH, A., Mécanique quantique (Dunod, Paris, 1959).